

Determining the Dependence Structure of Multivariate Extremes

E. S. Simpson¹, J. L. Wadsworth², J. A. Tawn²

¹*STOR-i Centre for Doctoral Training, Lancaster University, Lancaster, LA1 4YR, U.K.*

²*Department of Mathematics and Statistics, Lancaster University, Lancaster, LA1 4YF, U.K.*

Abstract

In multivariate extreme value analysis, the nature of the extremal dependence between variables should be considered when selecting appropriate statistical models. Interest often lies with determining which subsets of variables can take their largest values simultaneously, while the others are of smaller order. Our approach is based on exploiting hidden regular variation properties on a collection of non-standard cones. This provides a new set of indices that reveal aspects of the extremal dependence structure not available through any existing measures of dependence. We derive theoretical properties of these indices, demonstrate their value through a series of examples, and develop methods of inference which also estimate the proportion of extremal mass associated with each cone. We consider two inferential approaches: in the first, we approximate the cones via a truncation of the variables; the second involves partitioning the simplex associated with their radial-angular components. We apply the methods to UK river flows, estimating the probabilities of different subsets of sites being simultaneously large.

Keywords: asymptotic independence, extremal dependence structure, hidden regular variation, multivariate regular variation.

1 Introduction

When constructing models in multivariate extreme value analysis, we often need to exploit extremal dependence features. Consider the random vector $X = (X_1, \dots, X_d)$, with $X_i \sim F_i$, as well as a subset of these variables $X_C = (X_i : i \in C)$, for some $C \in 2^D \setminus \emptyset$, i.e., C is in the power set of $D = \{1, \dots, d\}$ without the empty set. For any C with $|C| \geq 2$, extremal dependence of the variables X_C can be summarized by

$$\chi_C = \lim_{u \rightarrow 1} \text{pr} \{F_i(X_i) > u : i \in C\} / (1 - u), \quad (1)$$

where we assume the limit exists. In particular, if $\chi_C > 0$, the variables in X_C are asymptotically dependent, i.e., can take their largest values simultaneously. If $\chi_C = 0$, the variables in X_C cannot all take their largest values together, although it is possible that for any $\underline{C} \subset C$, $\chi_{\underline{C}} > 0$, see for example Hua and Joe (2011) or Wadsworth and Tawn (2013).

Many models for multivariate extremes are only applicable when data exhibits either full asymptotic dependence, entailing $\chi_C > 0$ for all $C \in 2^D \setminus \emptyset$ with $|C| \geq 2$, or full asymptotic independence, i.e., $\chi_{i,j} = 0$ for all $i < j$, see Heffernan and Tawn (2004). However, it is often the case that some χ_C are positive whilst others are zero, i.e., only certain subsets of the variables take their largest values simultaneously, while the other variables are of smaller order. The extremal dependence between variables can thus have a complicated structure, which should be exploited when modelling. In this paper, we present two methods for determining this structure for a set of variables.

The full extremal dependence structure is not completely captured by the $2^d - d - 1$ coefficients $\{\chi_C : C \in 2^D \setminus \emptyset, |C| \geq 2\}$ since we do not learn fully about whether small values of some variables occur with large values of others, or if individual variables can be extreme in isolation. This is revealed most clearly by decomposing

the vector into radial and angular components, (R, W) , and examining their asymptotic structure. If the X_i follow a common heavy-tailed marginal distribution, usually achieved via a transformation, these pseudo polar coordinates are defined as $R = \|X\|_1$ and $W = X/\|X\|_2$, for arbitrary norms $\|\cdot\|_1$ and $\|\cdot\|_2$. We take both to be the L_1 norm, and assume that X has standard Fréchet margins, so that $\text{pr}(X_i < x) = \exp(-1/x)$ for $x > 0$ and $i = 1, \dots, d$. As such, the radial and angular components are $R = \sum_{i=1}^d X_i$ and $W = X/R$, respectively, with $R > 0$ and $W \in \mathcal{S}_{d-1} = \{(w_1, \dots, w_d) \in [0, 1]^d : \sum_{i=1}^d w_i = 1\}$, the $(d-1)$ -dimensional unit simplex. It follows that $\text{pr}(R > r) \sim ar^{-1}$ as $r \rightarrow \infty$, for $a \geq 1$, so all the information about extreme events is contained in W , and in particular the distribution of $W \mid R > r$ as $r \rightarrow \infty$. Under the assumption of multivariate regular variation (see e.g., Resnick (2010)),

$$\lim_{t \rightarrow \infty} \text{pr}(R > tr, W \in B \mid R > t) = H(B)r^{-1}, \quad (2)$$

for $r \geq 1$ and B a measurable subset of \mathcal{S}_{d-1} , where the limiting spectral measure H satisfies

$$\int_{\mathcal{S}_{d-1}} w_i dH(w) = 1/d, \quad i = 1, \dots, d. \quad (3)$$

As the radial component becomes large, the position of mass on \mathcal{S}_{d-1} reveals the extremal dependence structure of X . We note the link between the dependence measure χ_C in (1), and the spectral measure H : if $\chi_C > 0$, then H places mass on at least one region $\mathcal{S}_{d-1}^{\bar{C}} = \{(w_1, \dots, w_d) \in [0, 1]^d : \sum_{i \in \bar{C}} w_i = 1\}$, with $C \subseteq \bar{C} \subseteq D$. This highlights that the term asymptotic dependence is not so useful here, since it offers only partial insight into the structure. In what follows, we thus avoid this nomenclature where possible, talking instead about faces of the simplex on which H places mass.

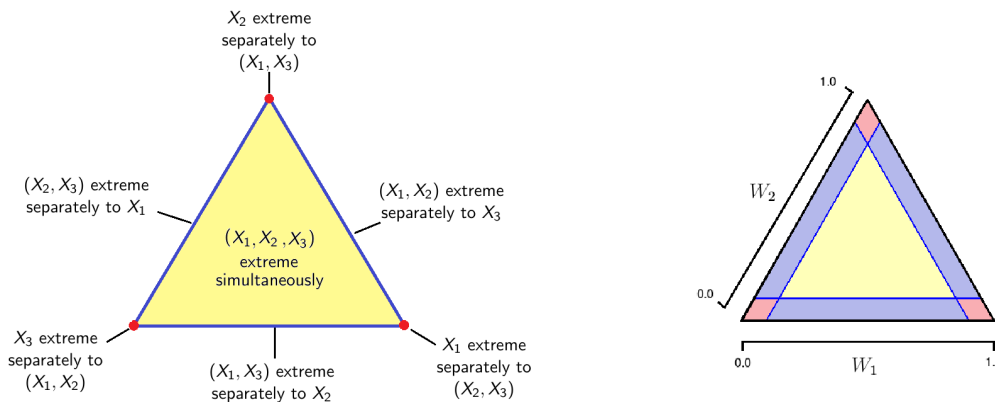


Figure 1: Left: the trivariate angular simplex, \mathcal{S}_2 . Right: a partition of \mathcal{S}_2 . The pink, blue and yellow regions represent the regions where exactly one, two or three of the variables are large, respectively.

In the d -dimensional case, \mathcal{S}_{d-1} can be partitioned into $2^d - 1$ faces, each of which could contain mass. Mass on each of these faces corresponds to a different subset of the variables (X_1, \dots, X_d) being the only ones taking their largest values concurrently. This is demonstrated in the left panel of Figure 1 for the case where $d = 3$. Here, and throughout the paper, the coordinates are transformed to the equilateral simplex for visual purposes. For high, or even moderate, dimensions, there are many faces to consider, and the task of determining which faces truly contain mass, and therefore the extremal dependence structure of the variables, is not straightforward, because for a finite sample with continuous margins, we will never observe points lying exactly on the boundary of the simplex. That is, no values of $W_i = 0$ when $R < \infty$.

The problem of determining the extremal dependence structure of variables has been recently studied elsewhere in the literature. Under the assumption that the data are from an elliptical copula, Klüppelberg et al. (2015) use factor analysis on extreme correlations linked to the tail dependence function. Chautru (2015) introduces a non-parametric approach based on statistical learning, combining a principal component analysis algorithm with clustering techniques. A Bayesian clustering method is proposed by Vettori et al. (2017), based

on the hierarchical dependence structure of the nested logistic distribution of Tawn (1990). Goix et al. (2016, 2017) propose a nonparametric simplex partitioning approach in which they condition on the radial variable being above some high threshold. They assume that there is mass on a particular face if the number of points in the corresponding region of the simplex is sufficiently large, leading to a sparse representation of the dependence structure. Chiapino and Sabourin (2017) propose an algorithm to group together nearby faces with extremal mass into feature clusters, by exploiting their graphical structure and a measure of extremal dependence. Finally, Chiapino et al. (2018) extend this approach by instead using the coefficient of tail dependence of Ledford and Tawn (1996).

In this paper we exploit additional, but commonly satisfied, hidden regular variation assumptions in regions of the angular simplex where H places no limiting mass. By considering hidden regular variation on non-standard cones, we introduce a new set of parameters that describes the dominant extremal dependence structure on the simplex. We study theoretical properties of these parameters, and explore their values for a range of examples. Estimation of the parameters provides us with an asymptotically-motivated framework for determining the extremal dependence structure, as well as allowing us to estimate the proportion of mass on each face. We propose two methods for doing this. In the first, we partition the cone in which X lives, rather than the simplex, whilst in the second we partition \mathcal{S}_{d-1} itself. The former has a more direct link to the theoretical motivation of Section 2; the latter provides a compromise between empirical estimation of H and exploitation of the new hidden regular variation assumptions. The computational complexity of both methods is $O(dn \log n)$, for d representing the number of variables and n the number of data points. This is the same complexity as the method proposed by Goix et al. (2017).

2 Theoretical motivation

2.1 Marginal distributions

We assume that the random vector $X = (X_1, \dots, X_d)$ has identically distributed margins, with a unit Fréchet tail, but probability $p > 0$ of being 0. That is,

$$\text{pr}(X_i < x) = \begin{cases} p, & 0 \leq x < -1/\log p, \\ e^{-1/x}, & x \geq -1/\log p, \end{cases} \quad (4)$$

for $i = 1, \dots, d$. As $x \rightarrow \infty$, $\text{pr}(X_i > x) \sim 1/x$, so the tail of (4) behaves asymptotically like a Pareto tail. Permitting this mass at zero allows us to consider cones representing regions where some values are large whilst others are small; see Section 2.3. It also alleviates some of the problems associated with X_i being continuous.

2.2 Multivariate regular variation

A function $\lambda : (0, \infty] \rightarrow (0, \infty]$ is said to be regularly varying at infinity, with index $\alpha \in \mathbb{R}$, if $\lambda(tx)/\lambda(t) \rightarrow x^\alpha$, as $t \rightarrow \infty$, for all $x > 0$. For such functions, we write $\lambda \in RV_\alpha$. We can always express $\lambda(x) = L(x)x^\alpha$, with $L \in RV_0$ termed a slowly varying function. A cone $G \subset \mathbb{R}^d$ is a set such that for any $x \in G$, $tx \in G$ for all $t > 0$. The assumption of multivariate regular variation on the cone G means that there exists a scaling function $a(t) \rightarrow \infty$ such that

$$t \text{ pr}(X/a(t) \in \cdot) \rightarrow \mu(\cdot), \quad (5)$$

with vague convergence in the space of non-negative Radon measures on G (see Resnick (2010), Chapter 3). If we assume that the margins of X are standard Fréchet or Pareto, or follow distribution (4), we may take $a(t) = t$, and the limit measure μ is homogeneous of order -1 .

2.3 Hidden regular variation

The concept of hidden regular variation was introduced by Resnick (2002), who formalized and extended the ideas of Ledford and Tawn (1996, 1997). Further work has been done by Maulik and Resnick (2004) and Mitra

and Resnick (2011), for example, whilst Resnick (2010) provides a textbook treatment. Here, multivariate regular variation is assumed on some cone in \mathbb{R}^d . If there is also regular variation, but with a scaling function of smaller order, on some sub-cone, we have hidden regular variation on that sub-cone.

Assumption 1. *We assume regular variation on the cone $\mathbb{E} = [0, \infty]^d \setminus \{0\}$, so that equation (5) is satisfied with μ homogeneous of order -1 , and consider sub-cones of the form*

$$\mathbb{E}_C = \{x \in \mathbb{E} : x_i \in (0, \infty], i \in C; x_j = 0, j \notin C\}, \quad (6)$$

where $C \in 2^D \setminus \emptyset$ for $D = \{1, \dots, d\}$. Such sub-cones represent regions where only variables X_i are large, for $i \in C$. On some such sub-cones, we could have scaling function $b_C(t) = t$ and $\mu(\mathbb{E}_C) > 0$, so that we have regular variation on \mathbb{E}_C where the limit measure is homogeneous of order -1 . Otherwise, $\mu(\mathbb{E}_C) = 0$ and we assume hidden regular variation, so that

$$t \operatorname{pr}(X/b_C(t) \in \cdot) \rightarrow \nu_{\tau_C}(\cdot) \quad (7)$$

converges vaguely on \mathbb{E}_C , with $b_C(t) = o(t) \in RV_{\tau_C}$, and ν_{τ_C} is homogeneous of order $-1/\tau_C$, for some $\tau_C \in (0, 1]$.

For $C \neq D = \{1, \dots, d\}$, \mathbb{E}_C is a non-standard choice of cone for hidden regular variation assumptions. Examining the regular variation properties of such cones leads to understanding of the sub-asymptotic behaviour of μ in relation to which of these sub-cones of \mathbb{E} are charged with mass. This is analogous to determining the support of H ; see Section 2.4. Das et al. (2013) also consider hidden regular variation on a series of non-standard cones from a theoretical viewpoint, although these are mostly different to the ones we consider. In the remainder of this section, we illustrate the utility and validity of the hidden regular variation assumption on cones \mathbb{E}_C via a series of examples, and discuss properties of the indices τ_C .

To our knowledge, the marginal case of this hidden regular variation framework is the only one previously exploited from a statistical perspective. For $X_C = (X_i : i \in C)$, Ledford and Tawn (1997) considered multivariate regular variation on \mathbb{E} and hidden regular variation on

$$\mathbb{E}_C^* = \{x \in \mathbb{E} : x_i \in (0, \infty], i \in C; x_j \in [0, \infty], j \notin C\}, \quad (8)$$

with limit measures on \mathbb{E}_C^* homogeneous of order $-1/\eta_C$, for $\eta_C \in (0, 1]$. As $\mathbb{E}_D^* = \mathbb{E}_D$, we have $\tau_D = \eta_D$, which need not be true for other sets $C \subset D$. Theorems 1 and 2 clarify some links between τ_C and η_C .

The value of τ_C in (7) does not depend on the choice of p in (4) for fixed p . Taking fixed p implies that those variables in $D \setminus C$ are not growing as the variables in C grow. If instead we are interested in the case where variables in C grow at rate $b_C(t)$, while those in $D \setminus C$ grow at a slower rate, we can consider $p = p_t$ to be a function of t , with $p_t \rightarrow 1$ at a suitable rate as $t \rightarrow \infty$. This in turn impacts upon the values of τ_C that arise in convergence (7). As a consequence, we specifically define τ_C as the values implied for p fixed, but we illustrate the varying p case in the Supplementary Material.

Examples of τ_C . In the Appendix and Supplementary Material, respectively, we calculate the value of τ_C , with $C \in 2^D \setminus \emptyset$, for a range of bivariate and multivariate copulas. For the bivariate case, we restrict our investigation to a subclass of bivariate extreme value distributions (Tawn, 1988) which covers all possible structures for limiting mass on the angular simplex, focussing on the case where the spectral density is regularly varying at 0 and 1. For multivariate cases there are many more possibilities, so we study examples of trivariate extreme value distributions (Tawn, 1990), which have $\chi_C > 0$ for at least one set $|C| \geq 2$, and two classes of copula which have $\chi_C = 0$ for all $|C| \geq 2$. The results are summarized here.

The bivariate extreme value distribution in standard Fréchet margins has distribution function of the form $F(x, y) = \exp\{-V(x, y)\}$ for some exponent measure

$$V(x, y) = 2 \int_0^1 \max\{w/x, (1-w)/y\} dH(w), \quad (9)$$

where H denotes the spectral measure defined in equation (3) on the unit simplex $[0, 1]$, and $x, y > 0$. Suppose that we apply transformation (4) to the margins. There are three interesting subspaces: $\{0\}$, $\{1\}$ and $(0, 1)$. The first (second) space corresponds to the second (first) variable taking its largest values while the first (second) variable is of smaller order, and the $(0, 1)$ space corresponds to the two variables being simultaneously large. Supposing that $H(\{0\}) = \theta_2 \in [0, 1/2]$ and $H(\{1\}) = \theta_1 \in [0, 1/2]$, the distribution places mass θ_2 , θ_1 , $\theta_{1,2} = 1 - (\theta_1 + \theta_2)$ in these respective subspaces. If $\theta_1 + \theta_2 = 1$, the variables are independent, and for $C = \{1, 2\}$, $\mu(\mathbb{E}_C) = \mu(\mathbb{E}_{1,2}) = 0$. In this case, all the limiting mass is placed on $\{0\}$ and $\{1\}$. Here, the limit (7) holds for $C = \{1\}, \{2\}$ and $\{1, 2\}$ with $\tau_1 = \tau_2 = 1$ and $\tau_{1,2} = \eta_{1,2} = 1/2$.

In contrast, when $\theta_1 + \theta_2 < 1$, $\mu(\mathbb{E}_{1,2}) > 0$ and $\tau_{1,2} = 1$, i.e., there is mass on the interior of the simplex. Again, $\tau_{1,2} = \eta_{1,2} = 1$. If $\theta_i > 0$ and limit (7) holds for $C = \{i\}$, it follows that $\tau_i = 1$, for $i = 1, 2$, and there is mass on the corresponding vertex of the simplex. However, when $\theta_1 = \theta_2 = 0$, there is no mass on either vertex, and additional assumptions are required for limit (7) to hold. We suppose that H is absolutely continuous on $(0, 1)$ with Lebesgue density $h(w) = dH(w)/dw$ satisfying $h(w) \sim c_1(1-w)^{s_1}$ as $w \rightarrow 1$, and $h(w) \sim c_2w^{s_2}$ as $w \rightarrow 0$, for $s_1, s_2 > -1$ and $c_1, c_2 \in \mathbb{R}$. In the Appendix, we show that for $i = 1, 2$, $\tau_i = (2 + s_i)^{-1}$, with $0 < \tau_i < 1$ if h is regularly varying at 0 ($i = 2$) or 1 ($i = 1$), with index $s_i > -1$. To help clarify this final case, consider the bivariate extreme value distribution with the logistic dependence structure (Tawn, 1988), with $V(x, y) = (x^{-1/\alpha} + y^{-1/\alpha})^\alpha$ and

$$h(w) = \frac{1}{2} (\alpha^{-1} - 1) \left\{ w^{-1/\alpha} + (1-w)^{-1/\alpha} \right\}^{\alpha-2} \{w(1-w)\}^{-1-1/\alpha}, \quad (10)$$

for $\alpha \in (0, 1)$. For this model $s_1 = s_2 = -2 + 1/\alpha$, and so $\tau_1 = \tau_2 = \alpha$.

In the trivariate case there are many more possibilities for combinations of faces with mass. In Table 1, we present the values of τ_C for five examples, identifying in each case τ_C on vertices, edges and the interior of the triangular simplex shown in the left panel of Figure 1.

	Copula	Vertices	Edges	Interior
(i)	Independence	$\tau_1 = \tau_2 = \tau_3 = 1$	$\tau_{1,2} = \tau_{1,3} = \tau_{2,3} = 1/2$	$\tau_{1,2,3} = 1/3$
(ii)	Independence and BEV (logistic)	$\tau_1 = \tau_2 = \alpha, \tau_3 = 1$	$\tau_{1,2} = 1, \tau_{1,3} = \tau_{2,3} = \alpha/(\alpha + 1)$	$\tau_{1,2,3} = 1/2$
(iii)	TEV (logistic)	$\tau_1 = \tau_2 = \tau_3 = \alpha$	$\tau_{1,2} = \tau_{1,3} = \tau_{2,3} = \alpha/2$	$\tau_{1,2,3} = 1$
(iv)	Inverted TEV (logistic)	$\tau_1 = \tau_2 = \tau_3 = 1$	$\tau_{1,2} = \tau_{1,3} = \tau_{2,3} = 2^{-\alpha}$	$\tau_{1,2,3} = 3^{-\alpha}$
(v)	Gaussian	$\tau_1 = \tau_2 = \tau_3 = 1$	$\tau_{i,j} = \left(1_2^T \Sigma_{i,j}^{-1} 1_2\right)^{-1} (*)$	$\tau_{1,2,3} = \left(1_3^T \Sigma^{-1} 1_3\right)^{-1}$

Table 1: Values of τ_C for various trivariate copulas, where BEV and TEV denote bivariate and trivariate extreme value copulas, respectively. For the Gaussian copula, $\Sigma_{i,j}$ denotes the submatrix of the covariance matrix Σ corresponding to variables i and j . For all logistic models the dependence parameter α satisfies $0 < \alpha < 1$, with larger α values corresponding to weaker dependence. Here, $1_d \in \mathbb{R}^d$ is a vector of 1s.

(*) Can be guaranteed provided $1 + \rho_C \neq \sum_{C': |C'|=2, C' \neq C} \rho_{C'}$; see Supplementary Material.

Cases (i)-(iii) in Table 1 are all special cases of the trivariate extreme value copula. Case (i) is the independence copula which has limit mass on the vertices only. For the d -dimensional independence copula, the index of hidden regular variation is m^{-1} for a face of dimension $m \leq d$. Case (ii) is the copula corresponding to variables (X_1, X_2) following a bivariate extreme value logistic distribution (10), independent of X_3 . Here all the limit mass is placed on one edge and the opposite vertex of the triangular simplex. Again, τ_C differs between faces, with a different value on the edge with mass than on the other two edges. The trivariate extreme value logistic model of case (iii) places all extremal mass on the interior, so that $\tau_{1,2,3} = 1$, and $\tau_C < 1$ for all C with $|C| < 3$. Since this is a symmetric model, the index of hidden regular variation is the same on all three vertices, and is also equal on each of the edges.

Both copulas (iv) and (v) place all their limiting mass on the vertices, but unlike the independence copula, they have sub-asymptotic dependence, reflected by the values of τ_C on edges and the interior, which are closer

to one than in the independence case. Case (iv) is the inverted trivariate extreme value copula (Ledford and Tawn, 1997), with a symmetric logistic dependence model. For the Gaussian copula, case (v), the value of τ_C for $|C| = 2, 3$ is controlled by the correlation matrix Σ , with the index of hidden regular variation on the edges not necessarily equal. In both cases (iv) and (v), the value of $\tau_{1,2,3}$ is always less than or equal to every τ_C with $|C| = 2$. Finally, $\tau_{1,2,3} = \eta_{1,2,3}$, with $\eta_{1,2,3}$ for the Gaussian copula given, for example, by Nolde (2014).

Properties of τ_C . Theorems 1 and 2 demonstrate the link between τ_C , defined through (7), and η_C .

Theorem 1. *Assume (hidden) regular variation on \mathbb{E}_C^* defined in (8), with scaling function $b_C^* \in RV_{\eta_C}$, and non-null limit measure ν_{η_C} . Further, for all $\bar{C} \subseteq D$ such that $\bar{C} \supseteq C$, assume (hidden) regular variation on $\mathbb{E}_{\bar{C}}$ with scaling function $b_{\bar{C}} \in RV_{\tau_{\bar{C}}}$, and non-null limit measure $\nu_{\tau_{\bar{C}}}$. Then $\eta_C = \max_{\bar{C}: C \subseteq \bar{C}} \tau_{\bar{C}}$.*

Proof. Since $\mathbb{E}_C^* = \cup_{\bar{C}: C \subseteq \bar{C}} \mathbb{E}_{\bar{C}}$, mass from the limit measure ν_{η_C} concentrates on at least one of these sub-cones. Mass on a sub-cone \bar{C}' implies $\tau_{\bar{C}'} = \eta_{\bar{C}'}$, whereas no mass on a sub-cone \bar{C}' implies $\tau_{\bar{C}'} \leq \eta_{\bar{C}'}$. The result follows. \square

Examples (iv) and (v) in Table 1 make use of the following theorem.

Theorem 2. *For all $C \in 2^D \setminus \emptyset$ with $|C| \geq 2$, assume (hidden) regular variation on \mathbb{E}_C and \mathbb{E}_C^* with scaling functions $b_C \in RV_{\tau_C}$ and $b_C^* \in RV_{\eta_C}$, and non-null limit measures ν_{τ_C} and ν_{η_C} . If $\eta_C > \eta_{\bar{C}}$ for all $C \subset \bar{C}$, then $\tau_C = \eta_C$.*

Proof. Since $\mathbb{E}_D = \mathbb{E}_D^*$, $\eta_D = \tau_D$, and by Theorem 1, for any set $C_{d-1} \subset D$ with $|C_{d-1}| = d - 1$, we have

$$\eta_{C_{d-1}} = \max(\tau_{C_{d-1}}, \tau_D) = \max(\tau_{C_{d-1}}, \eta_D).$$

Since $\eta_{C_{d-1}} > \eta_D$, $\eta_{C_{d-1}} = \tau_{C_{d-1}}$. Continuing, for any set $C_{d-2} \subset C_{d-1}$ with $|C_{d-2}| = d - 2$,

$$\eta_{C_{d-2}} = \max(\tau_{C_{d-2}}, \tau_{C_{d-1}}, \tau_D) = \max(\tau_{C_{d-2}}, \eta_{C_{d-1}}, \eta_D).$$

Again, since $\eta_{C_{d-2}} > \eta_{C_{d-1}} > \eta_D$ for all $C_{d-2} \subset C_{d-1}$, then $\eta_{C_{d-2}} = \tau_{C_{d-2}}$. The result follows by iteration for any set C with $|C| \geq 2$. \square

2.4 Radial-angular components

In the second of our statistical methods, we consider variables in terms of their radial and angular components, with a focus on the position of the mass of H , defined in (2), on the simplex. Define

$$\mathbb{B}_C = \{w \in \mathcal{S}_{d-1} : w_i \in (0, 1], i \in C; w_j = 0, j \notin C\},$$

to be the face of the simplex corresponding to $x \in \mathbb{E}_C$. The measure H places mass on \mathbb{B}_C if and only if μ , defined in (5), places mass on \mathbb{E}_C . Assuming regular variation on the cone \mathbb{E} , and hidden regular variation on \mathbb{E}_C , by equation (11) of Resnick (2002), for $(R, W) = (\|X\|, X/\|X\|)$, we have

$$\text{tpr} \{(R/b_C(t), W) \in \cdot\} \rightarrow s \rho_{\tau_C} \times S_C,$$

with vague convergence on the space of non-negative measures on $(0, \infty) \times \mathbb{B}_C$, for some constant $s \in (0, \infty)$, where S_C is a Radon measure on \mathbb{B}_C , and ρ_{τ_C} satisfies $\rho_{\tau_C}((r, \infty]) = r^{-1/\tau_C}$ for $r > 0$. A consequence of this is that on any relatively compact subset A_C of \mathbb{B}_C with $S_C(\partial A_C) = 0$ and $S_C(A_C) > 0$,

$$\text{pr}(R > b_C(t)r \mid R > b_C(t), W \in A_C) = \frac{\text{pr}(R > b_C(t)r \mid W \in A_C)}{\text{pr}(R > b_C(t) \mid W \in A_C)} \rightarrow r^{-1/\tau_C},$$

for $r \geq 1$, as $t \rightarrow \infty$. An analogous result holds under regular variation. From the definition of regular variation in Section 2.2, we see that $\text{pr}(R > r \mid W \in A_C) \in RV_{-1/\tau_C}$. As such, we have

$$\text{pr}(R > r \mid W \in A_C) = L_C(r)r^{-1/\tau_C}, \tag{11}$$

where L_C is a slowly varying function and $\tau_C \in (0, 1]$. In particular, the faces where $\tau_C = 1$ and $L_C(r) \not\rightarrow 0$ ($r \rightarrow \infty$), are those containing extremal mass, and correspond to subsets of variables that take their largest values simultaneously while the remaining variables are of smaller order.

If $H(\mathbb{B}_C) > 0$, where H is the limiting measure as defined in Section 1, then $\tau_C = 1$. Due to the moment constraint in equation (3), we have the condition that for every $i \in \{1, \dots, d\}$, there must be at least one set $C \in 2^D \setminus \emptyset$ with $i \in C$ such that $\tau_C = 1$. That is, in the set of faces of the angular simplex with limiting mass, each variable must be represented at least once.

3 Methodology

3.1 Introduction to methodology

We now introduce two approaches for determining the extremal dependence structure of a set of variables, as well as the proportion of extremal mass on each face of the angular simplex and the rate at which mass disappears from each face as the radial component tends towards infinity. In the first method we transform the variables to have distribution (4) by setting any values below some marginal threshold equal to zero. This transformation is analogous to the approach of Goix et al. (2017), who partition the non-negative orthant in a similar way, but we additionally exploit Assumption 1. An alternative on the radial-angular scale, analogous to Goix et al. (2016), is to partition the simplex by ‘thickening’ its boundaries. This is tantamount to setting thresholds beyond which angular components are considered zero, and motivates our use of the hidden regular variation assumption of equation (11) in these regions.

3.2 Method 1: truncating X

Obtaining variables with distribution (4) can be achieved by taking $X \sim \text{Fréchet}(1)$ and setting

$$X^* = \begin{cases} 0, & X \leq -1/\log p, \\ X, & X > -1/\log p, \end{cases} \quad (12)$$

where p represents the percentile at which we truncate. The cone $\mathbb{E} = \bigcup_{C \in 2^D \setminus \emptyset} \mathbb{E}_C$, with the components of the union disjoint and defined as in (6). We wish to partition \mathbb{E} with approximations to \mathbb{E}_C , by creating regions where components indexed by C are large and those not in C are small. This is achieved via regions of the form

$$E_C = \{x^* \in \mathbb{E} : x_i^* > -1/\log p, i \in C; x_j^* = 0, j \notin C\}. \quad (13)$$

Model specification and parameter estimation. We define the variable $Q = \min(X_i^* : X_i^* > 0, i = 1, \dots, d)$, for which

$$\text{pr}(Q > q \mid X^* \in E_C) \propto \text{pr}(X_i^* > q, i \in C; X_j^* = 0, j \notin C) = \text{pr}(X^* \in M_{C,q}),$$

where $M_{C,q} = \{x \in \mathbb{E} : x_i \in (q, \infty), i \in C; x_j = 0, j \notin C\}$. By Assumption 1, $\text{tpr}(X^*/b_C(t) \in M_{C,q}) \rightarrow \nu_{\tau_C}(M_{C,q})$, as $t \rightarrow \infty$, for $q > 0$, and

$$\text{pr}(X^* \in b_C(t)M_{C,q} \mid X^* \in b_C(t)M_{C,1}) = \frac{\text{tpr}(X^*/b_C(t) \in M_{C,q})}{\text{tpr}(X^*/b_C(t) \in M_{C,1})} \rightarrow \frac{\nu_{\tau_C}(M_{C,q})}{\nu_{\tau_C}(M_{C,1})} = \frac{\nu_{\tau_C}(qM_{C,1})}{\nu_{\tau_C}(M_{C,1})} = q^{-1/\tau_C},$$

by homogeneity of the measure ν_{τ_C} , for $q > 1$. Hence $\text{pr}(X^* \in M_{C,q}) \in RV_{-1/\tau_C}$. We therefore assume the model

$$\text{pr}(Q > q \mid X^* \in E_C) = K_C q^{-1/\tau_C}, \quad q > u_C, \quad (14)$$

for a high threshold u_C , with $\tau_C \in (0, 1]$ and $K_C > 0$ for all $C \in 2^D \setminus \emptyset$. Here, the usual slowly varying function L_C is replaced by the constant K_C as a modelling assumption, removing the possibility of having $L_C(t) \rightarrow 0$ as

$q \rightarrow \infty$.

Model (14) may be fitted using a censored likelihood approach. In particular, suppose we observe n_C values q_1, \dots, q_{n_C} of Q in region E_C . The corresponding censored likelihood associated with this region is

$$L_C(K_C, \tau_C) = \prod_{j=1}^{n_C} \left(1 - K_C u_C^{-1/\tau_C}\right)^{\mathbb{1}_{\{q_j \leq u_C\}}} \left(\frac{K_C}{\tau_C} q_j^{-1-1/\tau_C}\right)^{\mathbb{1}_{\{q_j > u_C\}}}, \quad (15)$$

with u_C a high threshold. Analytical maximisation of (15) leads to closed form estimates of (K_C, τ_C) , with the latter corresponding to the Hill estimate (Hill, 1975). In particular,

$$\hat{\tau}_C = \left(\sum_{j=1}^{n_C} \mathbb{1}_{\{q_j > u_C\}} \right)^{-1} \sum_{j=1}^{n_C} \mathbb{1}_{\{q_j > u_C\}} \log \left(\frac{q_j}{u_C} \right); \quad \hat{K}_C = \left(\frac{\sum_{j=1}^{n_C} \mathbb{1}_{\{q_j > u_C\}}}{n_C} \right) u_C^{1/\hat{\tau}_C}. \quad (16)$$

This estimate of τ_C can be greater than 1, so in practice we estimate it as $\tilde{\tau}_C = \min(\hat{\tau}_C, 1)$, with an appropriate change to \hat{K}_C . The Hill estimator for τ_C is consistent under the standard conditions $u_C \rightarrow \infty$, $\sum_j \mathbb{1}_{\{q_j > u_C\}} \rightarrow \infty$ and $\sum_j \mathbb{1}_{\{q_j > u_C\}}/n_C \rightarrow 0$; the assumption of $L_C(t) \sim K_C > 0$ is not required for this. The second condition ensures that the number of points in E_C with $Q > u_C$ goes to infinity, and since the expected number $n_C \text{pr}(Q > u_C | X^* \in E_C) \sim n_C K_C u_C^{-1/\tau_C}$, this entails $u_C = o(n_C^{\tau_C})$.

A model for the proportion of mass in each region. The method proposed by Goix et al. (2017) essentially produces empirical estimates of $\text{pr}(X \in E_C | R > r_0)$, for $R = \|X\|_\infty$, and some value of r_0 within the range of observed values, intended to approximate the limit. In contrast, our proposed semiparametric method allows us to estimate $\text{pr}(X \in E_C | Q > q)$, where q may be larger than any observed value of Q ; in principle this allows us to get closer to the limit distribution that we are aiming to estimate. This is achieved by considering probabilities of the form

$$\text{pr}(X^* \in E_C | Q > q) = \frac{\text{pr}(Q > q | X^* \in E_C) \text{pr}(X^* \in E_C)}{\sum_{C' \in 2^D \setminus \emptyset} \text{pr}(Q > q | X^* \in E_{C'}) \text{pr}(X^* \in E_{C'})} \quad (17)$$

for $C \in 2^D \setminus \emptyset$ and E_C as in (13). Here, the denominator is $\text{pr}(Q > q, X^* \in \mathbb{E}) \sim a q^{-1}$, as $q \rightarrow \infty$, but we use the expression given to ensure our estimates of $\text{pr}(X \in E_C | Q > q)$ sum to one over $C \in 2^D \setminus \emptyset$.

The right hand side of equation (17) consists of two types of component. We estimate terms of the form $\text{pr}(X^* \in E_C)$ empirically, and those of the form $\text{pr}(Q > q | X^* \in E_C)$ are estimated as in (14) by replacing the values of K_C and τ_C by their estimates, and evaluating for some large q ; choice of q is discussed in Section 5. This approach yields an estimate for the proportion of mass in each region. We denote the estimated vector of these proportions as $\hat{p} = (\hat{p}_C : C \in 2^D \setminus \emptyset)$. In order to obtain a sparse representation of the mass on the simplex, we follow Goix et al. (2016, 2017) and ignore any mass that has been detected which is considered to be negligible; see item 4 below. In Section 2.3, we noted that, theoretically, $\max_{C: C \supseteq i} \tau_C = 1$ for all $i = 1, \dots, d$. This property is not guaranteed by our methods when fitting model (14), and presents a possible avenue for future work.

Summary of method.

1. Transform data to standard Fréchet margins, and for a choice of the tuning parameter p , apply transformation (12).
2. Assign each transformed observation to a region E_C as in (13), removing any all-zero points.
3. For each region E_C containing more than m points, fit model (14) using parameter estimates in (16) for a choice of threshold u_C , and estimate $\text{pr}(X^* \in E_C | Q > q)$ for a large value of q by equation (17). Set $\text{pr}(X^* \in E_C | Q > q) = 0$ in the remaining regions. Denote the resulting estimate by \hat{p}_C .

4. If $\hat{p}_C < \pi$, for a choice of the tuning parameter π , set \hat{p}_C to zero, renormalizing the resulting vector.

The parameter m in step 3 ensures there are sufficient points to estimate the parameters on each face. In simulations, it was found not have a significant effect on results, so we take the default choice $m = 1$.

3.3 Method 2: partitioning W

An alternative to applying transformation (12) to approximate mass on the boundaries of the angular simplex is to partition the simplex itself. The simplex \mathcal{S}_{d-1} is equivalent to the disjoint union $\bigcup_{C \in 2^D \setminus \emptyset} \mathbb{B}_C$. In an analogous way to the regions E_C in Method 1, we create approximations to \mathbb{B}_C using regions

$$B_C = \{w : w_i \geq 1 - \epsilon, i \in C; w_j < \epsilon, j \notin C\}, \quad (18)$$

for some small $\epsilon \in (0, 1/d]$. The right panel of Figure 1 gives an example of this partition in the trivariate case with $\epsilon = 0.1$.

In a similar manner to equation (17) in Method 1, for radial-angular components defined via the L_1 norm, we now consider probabilities of the form

$$\text{pr}(W \in B_C \mid R > r) = \frac{\text{pr}(R > r \mid W \in B_C)\text{pr}(W \in B_C)}{\sum_{C' \in 2^D \setminus \emptyset} \text{pr}(R > r \mid W \in B_{C'})\text{pr}(W \in B_{C'})}, \quad (19)$$

for $C \in 2^D \setminus \emptyset$ and B_C as in (18). Also analogously to Method 1, we estimate terms $\text{pr}(W \in B_C)$ empirically, and for the remaining terms use hidden regular variation assumption (11), supposing

$$\text{pr}(R > r \mid W \in B_C) = K_C r^{-1/\tau_C}, \quad \text{for } r > u_C. \quad (20)$$

Whilst the regular variation assumption is likely to be reasonable, in contrast to Section 3.2, the true indices of regular variation may not be τ_C in this case. Instead, the index will be $\tau_{\bar{C}}$ on B_C if $C \subset \bar{C}$ and $\tau_{\bar{C}} > \tau_C$, assuming $\nu_{\tau_{\bar{C}}}(\mathbb{B}_{\bar{C}} \cap B_C) > 0$, because the approximation B_C to \mathbb{B}_C includes parts of the true $\mathbb{B}_{\bar{C}}$. For example, in the trivariate case where all mass is in $\mathbb{B}_{1,2,3}$, or equivalently the centre of \mathcal{S}_2 , since $B_C \cap \mathbb{B}_{1,2,3} \neq \emptyset$ for all C with $|C| \leq 2$ (see Figure 1), in practice for fixed ϵ , $\text{pr}(R > r \mid W \in B_C) \in RV_{-1}$. In contrast, when all mass is on $\mathbb{B}_1, \mathbb{B}_2, \mathbb{B}_3$, i.e., the vertices of \mathcal{S}_2 , then assumption (20) is correct with the true τ_C values. In practice, Method 2 often estimates a less sparse set of faces than Method 1, which seems likely to be a consequence of this feature. Overall, Method 2 relies on a mixture of the regular variation assumption and empirical estimation. We investigate its relative performance in Section 4.

The estimates of (K_C, τ_C) in Method 2 are again obtained via a censored likelihood approach. Once the data have been transformed to radial-angular components and partitioned according to (18), the remaining steps of Method 2 are equivalent to 3, 4 and 5 in Method 1.

4 Simulation study

4.1 Overview and metrics

We present simulations to demonstrate Methods 1 and 2, and compare with the approach of Goix et al. (2017). Here, we consider the asymmetric logistic distribution of Tawn (1990), whilst in the Supplementary Material we present results for a max-mixture distribution involving bivariate Gaussian and extreme value logistic distributions. We test the efficacy of the methods as classifiers using receiver operating characteristic (ROC) curves, as well as an extension of these which we term ROC* curves. For the classes of model we consider, it is possible to analytically calculate the proportion of extremal mass on the various faces of the angular simplex, allowing us to compare the estimates from our methods to the true distribution of mass; we use the Hellinger distance for this.

When incorporating a cut-off for sparse representation of the spectral measure H , as mentioned in Section 3.2, the methods can be viewed as classification techniques. Plotting ROC curves is a common method for testing the efficacy of classifiers, see for example Hastie et al. (2009). To obtain such curves, the false positive rate of a method is plotted against the true positive rate, as some parameter of the method varies. In our case, the false positive rate is the proportion of faces incorrectly detected as having mass, while the true positive rate is the proportion of correctly detected faces. To obtain our curves, we vary the threshold, π , above which estimated mass is considered significant. For $\pi = 0$, all faces will be included in the estimated dependence structure, leading to the true and false positive rates both being 1, while $\pi = 1$ includes none of the faces, with the true and false positive rates both 0. A perfect result for a given data set and method would be a false positive rate of 0 and true positive rate of 1: the closer the ROC curve is to the point $(0, 1)$, the better the method. This is often quantified using the area under the curve (AUC), with values closer to 1 corresponding to more successful classification.

By using ROC curves, we can only test whether or not the faces determined as having mass are correct, giving a reasonably strict assessment of the methods. We may also wish to take into account faces detected as having mass that are close to the truth. We therefore propose an extension of the ROC curve, which we term the ROC* curve, that takes into account mass on adjacent faces. For the face corresponding to the set C , we define adjacent faces as those corresponding to any sets \underline{C} and \overline{C} with $\underline{C} \subset C \subset \overline{C}$ such that $|\underline{C}| = |C| - 1$ and $|\overline{C}| = |C| + 1$. When constructing ROC* curves, in place of the true positive rate, we consider the proportion of faces that should be detected which are either detected or have an adjacent face that is detected. The false positive rate is replaced by the proportion of faces that do not truly have mass and are not adjacent to any of the true faces with mass, that are detected as having mass. Interpretation of ROC* curves is analogous to that of standard ROC curves, and one may also consider the area under the ROC* curve (AUC*) as a measure for the success of the classifier.

Let $p = (p_C; C \in 2^D \setminus \emptyset)$ denote the true proportion of mass on each face, and denote its estimate by \hat{p} . The Hellinger distance between p and \hat{p} is defined as

$$HD(p, \hat{p}) = \frac{1}{\sqrt{2}} \left\{ \sum_{C \in 2^D \setminus \emptyset} \left(p_C^{1/2} - \hat{p}_C^{1/2} \right)^2 \right\}^{1/2}, \quad (21)$$

and is used to determine the precision of the estimated proportions. In particular, $HD(p, \hat{p}) \in [0, 1]$, and is 0 if and only if $p = \hat{p}$. The closer $HD(p, \hat{p})$ is to 0, the better p is estimated by \hat{p} . Errors on small proportions are penalized more heavily than errors on large proportions. If there is truly some small, non-zero mass on a particular region, which is estimated as zero, this will incur a relatively heavy penalty.

4.2 Asymmetric logistic distribution

In standard Fréchet margins, the multivariate extreme value (MEV) distribution function is of the form $\exp\{-V(x)\}$. Coles and Tawn (1991) show that the spectral density on the face corresponding to only variables $\{X_i : i \in C\}$ being concurrently large is $h_C(w_C) = -V^{\{C\}}(w_C)/d$, where

$$V^{\{C\}}(x_C) = \lim_{x_j \rightarrow 0: j \notin C} \left(\prod_{i \in C} \frac{\partial}{\partial x_i} \right) V(x),$$

for $x_C = \{x_i : i \in C\}$, $w_C = x_C/r_C$ and $r_C = \sum_{i \in C} x_i$. Hence the proportion of mass on that face is

$$p_C = -\frac{1}{d} \int_{\mathbb{B}_C} V^{\{C\}}(w_C) \prod_{i \in C} dw_i. \quad (22)$$

For the asymmetric logistic model (Tawn, 1990), the exponent measure V is defined as

$$V(x) = \sum_{C \in 2^D \setminus \emptyset} \left\{ \sum_{i \in C} (\theta_{i,C}/x_i)^{1/\alpha_C} \right\}^{\alpha_C}, \quad (23)$$

for $\theta_{i,C} \in [0, 1]$, with $\theta_{i,C} = 0$ if $i \notin C$, $\sum_{C \in 2^D \setminus \emptyset} \theta_{i,C} = 1$ for all $i = 1, \dots, d$, and $C \in 2^D \setminus \emptyset$, and dependence parameters $\alpha_C \in (0, 1]$. In Proposition 1 of the Supplementary Material, we show that for the d -dimensional asymmetric logistic model with all $\alpha_C \equiv \alpha$, the proportion of mass on face C is

$$p_C^{(d)} = \sum_{i \in C} \theta_{i,C} / d,$$

for any set $C \in 2^D \setminus \emptyset$. Using this new result, we can compare our estimated proportions to the truth using the Hellinger distance defined in (21).

Following the approach of Goix et al. (2017), we simulate data from an asymmetric logistic distribution with $\alpha_C \equiv \alpha$, whose extremal mass is concentrated on f randomly chosen faces, ensuring that moment constraint (3) is satisfied. Suppose the faces chosen correspond to subsets $F_1, \dots, F_f \in 2^D \setminus \emptyset$. The conditions on the parameters of the asymmetric logistic distribution are satisfied by setting

$$\theta_{i,C} = |\{j : i \in F_j, j \in \{1, \dots, f\}\}|^{-1}, \quad (24)$$

for $C \in \{F_1, \dots, F_f\}$, and $\theta_{i,C} = 0$ otherwise.

Each setting in the simulation study is repeated 100 times. In Method 1, we set $p = 0.5$, u_C to be the 0.75 quantile of observed Q values in region E_C for each $C \in 2^D \setminus \emptyset$, and the value of q for which we estimate $\text{pr}(X^* \in E_C \mid Q > q)$ to be the 0.9999 quantile of all observed Q values. In Method 2, we set $\epsilon = 0.05$, each threshold u_C to be the 0.975 quantile of observed radial values over all sets $C \in 2^D \setminus \emptyset$, and r in $\text{pr}(W \in B_C \mid R > r)$ to be the largest observed radial value for the particular sample. The parameters in the method of Goix et al. (2017) are chosen to be $(\epsilon, k) = (0.1, \sqrt{n})$, using notation from that paper. When calculating the Hellinger distances, we used $\pi = 0.001$ as the value above which estimated mass is considered significant in all three methods. The tuning parameters are not optimized for individual data sets, but fixed at values that we have found to work well across a range of settings. In Section 4.3, we discuss stability plots, which could be used as guide as to which tuning parameter values may be sensible for a given set of data. In Section 5, we present tables showing how the estimated extremal dependence structure changes as the tuning parameters vary for a particular data set, allowing us to further examine this mass stability and choose a reasonable value of p in Method 1 or ϵ in Method 2.

We present results for dimensions $d = 5$ and $d = 10$. For $d = 5$, we simulate samples of size $n = 10,000$, and test both our methods when there are truly 5, 10 and 15 faces with extremal mass. For $d = 10$, we have $n = 100,000$ samples, and consider 10, 50 and 100 faces with extremal mass. In Table 2, we present the average AUC for $\alpha \in \{0.25, 0.5, 0.75\}$. Boxplots of the full results obtained are provided in the Supplementary Material. In the asymmetric logistic model, the closer α_C is to 1, the larger the values of τ_C for $\underline{C} \subset C$, as demonstrated by cases (ii) and (iii) in Table 1. Thus, the larger the value of α in our simulations, the more difficult it is to determine which faces truly contain extremal mass. In Figure 2, we present AUC* values, as defined in Section 4.1, for the same 5-dimensional cases as above, but only consider $\alpha = 0.75$, where classification is most difficult. If every face without mass has at least one neighbouring face truly having mass, the false positive rate, and hence the AUC* value, will always be zero; these cases have been removed in Figure 2.

The average AUC values in Table 2 show that all three methods perform well when $\alpha = 0.25$ and $\alpha = 0.5$, for both $d = 5$ and $d = 10$. The results suggest that the method of Goix et al. (2017) is generally the most successful classifier when $\alpha = 0.75$, closely followed by Method 1; this is supported by the boxplots of the results in the Supplementary Material. It is possible that the method of Goix et al. is most successful for larger values of α since it is more difficult for Methods 1 and 2 to distinguish between regions where τ_C does and does not equal 1 in these cases. For the AUC* results in Figure 2, Method 2 outperforms Method 1 in all cases. The method of Goix et al. also performs well under the AUC* criteria, although Method 2 is the most successful for $f = 10$ and $f = 15$. This suggests that the extremal dependence structures estimated using Method 2 are

(α, f)	(0.25, 5)	(0.25, 10)	(0.25, 15)	(0.5, 5)	(0.5, 10)	(0.5, 15)	(0.75, 5)	(0.75, 10)	(0.75, 15)
Goix et al.	1.000	0.998	0.994	0.999	0.997	0.994	0.985	0.925	0.868
Method 1	1.000	1.000	1.000	1.000	1.000	0.999	0.924	0.886	0.846
Method 2	0.999	0.997	0.991	0.994	0.981	0.960	0.937	0.885	0.803

(α, f)	(0.25, 10)	(0.25, 50)	(0.25, 100)	(0.5, 10)	(0.5, 50)	(0.5, 100)	(0.75, 10)	(0.75, 50)	(0.75, 100)
Goix et al.	1.000	1.000	1.000	1.000	1.000	0.998	0.995	0.988	0.969
Method 1	1.000	1.000	1.000	1.000	1.000	0.999	0.996	0.985	0.960
Method 2	1.000	1.000	0.999	1.000	0.995	0.981	0.985	0.931	0.878

Table 2: Average AUC values for 100 samples from 5-dimensional (top) and 10-dimensional (bottom) asymmetric logistic distributions, with dependence parameter α and $\theta_{i,C}$ determined via (24).

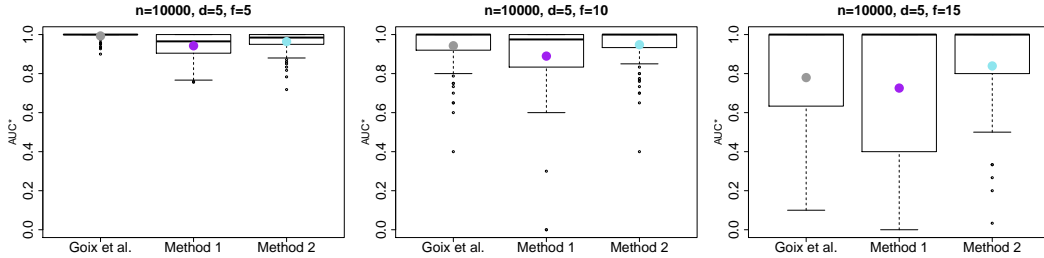


Figure 2: Boxplot of AUC^* values for $d = 5$; $f = 5, 10, 15$; $n = 10,000$ and $\alpha = 0.75$. Average AUC^* values are shown by the circles in each plot.

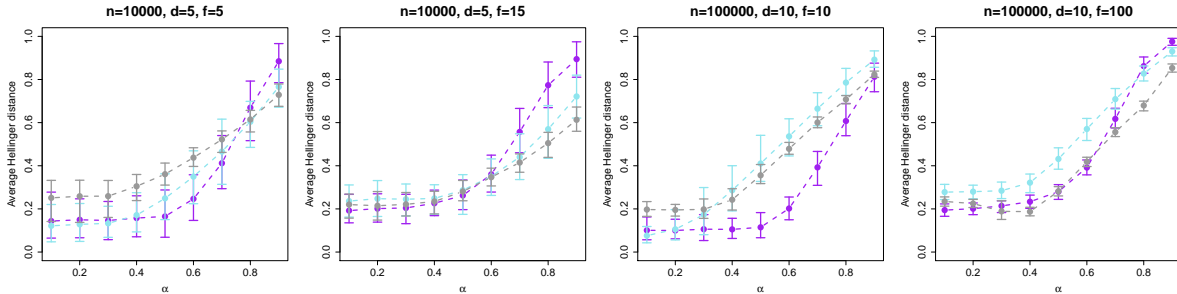


Figure 3: Mean Hellinger distance, 0.05 and 0.95 quantiles over 100 simulations. Method 1: purple; Method 2: blue; Goix et al.: grey.

often close to the truth, even when these are expected to be particularly difficult to detect.

Figure 3 shows the average Hellinger distance for $\alpha \in [0.1, 0.9]$ for four of the cases described above: the remaining two cases are presented in the Supplementary Material. The three methods perform similarly well when f is large. For the more sparse cases, $(d, f) = (5, 5)$ and $(d, f) = (10, 10)$, overall Method 1 performs significantly better than the other two approaches. When the extreme values are concentrated on fewer faces, it may be easier to estimate true values of $\tau_C = 1$ using Method 1 than in less sparse examples. For the asymmetric logistic distribution, the method of Goix et al. (2017) often performs better in terms of classification, while Method 1 is better at estimating the proportion of extremal mass on each face. In the Supplementary Material, we present results for a max-mixture distribution, where Method 2 is the most successful method overall, particularly in terms of the average Hellinger distance.

4.3 Stability plots

A possible way to decide on reasonable tuning parameter values for a given set of data is to use parameter stability plots. Here, we outline how to construct such a plot for an example using the asymmetric logistic

distribution with Method 2, where our aim is to obtain a sensible range of values for the tuning parameter ϵ , by considering the region of ϵ where the number of faces determined as having mass is stable.

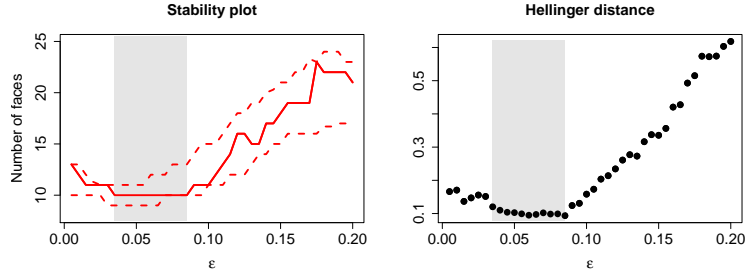


Figure 4: Stability plot (left) for Method 2, with dashed lines showing a 95% bootstrapped confidence interval for the number of faces with mass, and a plot of the Hellinger distance (right) for each value of ϵ . The shaded regions correspond to the stable range of tuning parameter values. Data were simulated from an asymmetric logistic distribution with $n = 10,000$, $d = 5$, $f = 10$ and $\alpha = 0.25$.

For $\epsilon \in \{0.005, 0.01, \dots, 0.2\}$, we use Method 2 to estimate the proportion of extremal mass on each face of the simplex, and find the number of faces whose estimated mass is greater than $\pi = 0.001$ in each case. The remaining parameters are fixed as in Section 4.2. Figure 4 shows the estimates of the number of faces, with a 95% confidence interval constructed from 250 bootstrapped samples: these constitute our stability plot. Analogous plots can be created to choose p in Method 1, or in each case to choose π . In practice, the choice of threshold π should depend on the dimension of the data; this is not explored here.

The number of faces detected as having mass is most stable for values of ϵ between 0.035 and 0.085, indicated by the shaded regions in Figure 4, suggesting values of ϵ in this range may be appropriate for this sample. Values of ϵ within the stable range correctly suggest there are ten faces with mass. The right panel of Figure 4 shows the Hellinger distance corresponding to the set of estimated proportions obtained for each value of ϵ . For this particular sample, the Hellinger distance is lowest for values of ϵ within the stable range, and is reasonably consistent across these tuning parameter values. In practice, the true proportions on each face are unknown, so Hellinger plots cannot be constructed; here it supports the idea of using stability plots in choosing suitable tuning parameter values. While there is no guarantee that stability plots will find the optimal tuning parameter values, they do offer a partial insight into the complex problem of tuning parameter optimization. Consideration of the context of the problem may be useful in determining whether it is reasonable for extremal mass to be placed on particular combinations of faces.

5 River flow data

We apply Methods 1 and 2 to daily mean river flow readings from 1980 to 2013, measured in cubic metres per second, at five gauging stations in the North West of England. These data are available from the Centre for Ecology and Hydrology (CEH) at nrfa.ceh.ac.uk (Morris and Flavin, 1990, 1994). Estimates of the extremal dependence structure of the flows could be used to aid model selection, or one could carry out density estimation on each face to give an overall model. The locations of the five gauges are shown in Figure 5; the labels assigned to each location will be used to describe the dependence structures estimated in this section. Figure 5 also illustrates the boundaries of the catchments associated with each gauge; these data are also available from CEH. These catchments demonstrate the areas from which surface water, usually as a result of precipitation, will drain to each gauge. The spatial dependence of river flow is studied by Keef et al. (2013) and Asadi et al. (2015). As high river flow is mainly caused by heavy rainfall, we may observe extreme river flow readings at several locations simultaneously if they are affected by the same extreme weather event. Gauges with adjacent or overlapping catchments are expected to take their largest values simultaneously, with stronger dependence

between gauges that are closer together.

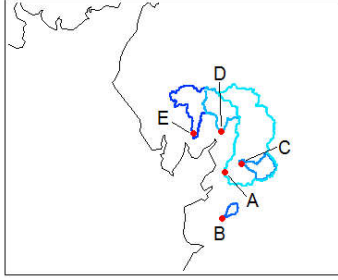


Figure 5: Locations of the river flow gauges (labelled A to E) and corresponding catchment boundaries.

Table 3 shows the percentage of the extremal mass assigned to each face of the angular simplex for tuning parameter values $p \in \{0.7, 0.725, \dots, 0.975\}$ (Method 1) and $\epsilon \in \{0.01, 0.015, \dots, 0.065\}$ (Method 2). We set $\pi = 0.01$ to be the threshold below which the proportion of mass is deemed negligible, and the extrapolation levels q and r in (17) and (19) to be the 0.999 quantile of the observed Q and R values in Methods 1 and 2, respectively. Remaining parameters are fixed as in Section 4.2. By observing how the estimated dependence structure changes over a range of tuning parameter values, we aim to find a ‘stable region’ in which the results are most reliable, indicated by the blue shaded regions in Table 3.

p	B	C	E	AD	BC	DE	ABC	ABD	ACD	ADE	ABCD	ABDE	ACDE	ABCDE
0.700	2										3			95
0.725	2										4			93
0.750	1										4			95
0.775	1										11			88
0.800	7										11			82
0.825	10	3									16			71
0.850	13	7									17			63
0.875	12	12									19		1	55
0.900	8	31									15			46
0.925	6	57					2			2	15			19
0.950	5	52					4			2	16			21
0.975	14	1	73	2	1								2	6

ϵ	B	C	E	AD	BC	DE	ABC	ABD	ACD	ADE	ABCD	ABDE	ACDE	ABCDE
0.010						1	5		2	3	29			9
0.015			2		2		8		1	7	36			16
0.020			2		1	3	10		2	7	39			18
0.025			4		1	3	12		4	5	39			18
0.030			5		2	4	13		5	6	38			17
0.035	1		5	2	2	6	15		6	5	35			15
0.040	1		8	2	2	5	19	1	9	6	21			15
0.045	2	8	3	2	6	19	2	9	7	19	14	11		11
0.050	2	10	3	3	3	18	2	9	7	18	14	10		10
0.055	2	10	4	3	4	19	1	10	9	22	9	8		8
0.060	2	9	4	6	5	17		10	9	25	9	5		5
0.065	2	10	5	6	6	16		10	10	24	2	8		2

Table 3: The percentage of mass assigned to each face for varying values of the tuning parameters in Method 1 (left) and Method 2 (right). The blue regions demonstrate the stable ranges, and the bold rows show our chosen tuning parameter value in each case.

Focussing on tuning parameter values within each of the stable regions in Table 3, Method 1 suggests the dependence structure to be $\{B, E, ABCD, ABCDE\}$, while Method 2 suggests $\{B, E, AD, BC, DE, ABC, ABD, ACD, ADE, ABCD, ACDE, ABCDE\}$. This demonstrates that Method 2 tends to estimate mass on more faces than Method 1, as discussed in Section 3.3. In Table 3, we fixed the value of q or r at a quantile of the observed Q or R values. None of the estimated τ_C values for Method 1 were exactly 1, and were generally lower than for Method 2. The extrapolation step therefore produced more faces with zero-mass in Method 1 than Method 2. If we had used a higher threshold for the negligible mass, say $\pi = 0.1$, for tuning parameter values in the stable region, Method 1 would have detected mass on faces $\{B, ABCD, ABCDE\}$ while the suggested structure using Method 2 would have been $\{ABC, ABCD, ACDE, ABCDE\}$. In this case, all the faces detected by Method 2 are either also detected by Method 1, or are neighbours of faces detected by Method 1, showing there is some agreement between the methods. We also investigated the behaviour of the methods using the 0.99 and 0.9999 quantiles for q and r in (17) and (19). For both methods, the set of faces estimated as having mass was stable, but for the lower quantile we found that Method 2 placed more mass on faces ABCD, ACDE and ABCDE, while more of the mass was estimated on face ABCDE for Method 1 when using a higher quantile.

The subsets of locations detected as having simultaneously high river flows seem feasible when considering the geographic positions of the gauging stations. For instance, both methods suggest mass on ABCD; as station E lies towards the edge of the region under consideration, it is possible for weather events to affect only the

other four locations. The catchment of gauge C lies entirely within the catchment of gauge A. We observe that locations C usually occurs with location A in the subsets of sites determined to take their largest values simultaneously, which is likely to be a consequence of this nested structure.

p	B	C	AD	BC	ABC	ABD	ACD	BCD	ABCD
0.700									100
0.725									100
0.750									100
0.775									100
0.800									100
0.825	3								97
0.850	3								97
0.875	4								96
0.900	2								98
0.925	5				1				94
0.950	7		2		5		2		84
0.975	35	3	1	2			7		52

ϵ	B	C	AD	BC	ABC	ABD	ACD	BCD	ABCD
0.010					3		2		95
0.015			2	1	6		5		86
0.020			2	1	9		6		82
0.025			3	2	12		12		72
0.030			3	3	13		16		65
0.035	1		4	2	16		18		58
0.040	1		6	2	21	1	23		46
0.045	1		5	3	22	2	24		43
0.050	2		5	4	21	3	25		41
0.055	2		6	4	22	3	25		39
0.060	2		6	6	20	2	25		39
0.065	2		7	7	19	1	25	1	38

Table 4: Estimated percentage of extremal mass on to each face when considering locations A-D, for varying values of the tuning parameters in Method 1 (left) and Method 2 (right).

To assess whether our methods are self-consistent across different dimensions, in Table 4 we present similar results for locations A, B, C and D. We would expect the subsets of locations deemed to be simultaneously large to be the same as in Table 3 if we ignore location E. Indeed, the combinations of sites in this four-dimensional example that are most consistently detected as having mass are $\{B, ABCD\}$ for Method 1 and $\{B, AD, BC, ABC, ABD, ACD, ABCD\}$ for Method 2, all of which occurred in the five-dimensional case either in their own right or with the addition of location E.

Tables 3 and 4 demonstrate the importance of tuning parameter selection in Methods 1 and 2. As p or ϵ increase, we are more likely to detect mass on the corner regions of the simplex, or faces corresponding to subsets of the variables with low cardinality. Likewise, for low values of p or ϵ , we assign more extremal mass to the centre of the angular simplex. In practice, there is often a reasonable degree of stability in the regions determined to have extremal mass as p or ϵ vary. Our methods could be used to impose structure in more complete models for multivariate extremes. Even if a handful of different options look plausible with some variation in p or ϵ , this is still a huge reduction over the full set of possibilities.

Appendix

A Calculation of τ_C for a bivariate extreme value distribution

We define variables with distribution (4) by applying truncation (12), denoted X_i^* for $i = 1, 2$. Since $b_C(t)$ in (7) is regularly varying with index τ_C , its value is determined by finding $b_C(t)$ such that

$$\text{pr} \{X_i^*/b_C(t) > x_i, i \in C; X_i^*/b_C(t) = 0, i \notin C\} \asymp t^{-1}$$

as $t \rightarrow \infty$, with $x_i > 0$ for $i = 1, 2$. Here, we calculate τ_1 , τ_2 and $\tau_{1,2}$ for a bivariate extreme value distribution, with distribution function given in (9). The exponent measure V can be written as

$$V(x, y) = \frac{2}{y} \int_0^1 (1-w)dH(w) - \frac{2}{y} \int_{\frac{x}{x+y}}^1 (1-w)h(w)dw + \frac{2}{x} \int_{\frac{x}{x+y}}^1 wh(w)dw + \frac{2\theta_1}{x}.$$

To study τ_1 , the rate on endpoint $\{1\}$ of the angular simplex, suppose that $h(w) \sim c_1(1-w)^{s_1}$ as $w \rightarrow 1$, for $s_1 > -1$. For $x \rightarrow \infty$ and $y = o(x)$, applying Karamata's theorem, we have

$$\begin{aligned} V(x, y) &= \frac{1}{y} - \frac{2c_1}{y(s_1+2)} \left(\frac{y}{x+y}\right)^{s_1+2} \{1+o(1)\} + \frac{2c_1}{x(s_1+1)} \left(\frac{y}{x+y}\right)^{s_1+1} \{1+o(1)\} + \frac{2\theta_1}{x} \\ &= \frac{1}{y} + 2c_1 \left(\frac{y}{x+y}\right)^{s_1+1} \left\{ \frac{1}{x(s_1+1)} - \frac{1}{(s_1+2)(x+y)} \right\} \{1+o(1)\} + \frac{2\theta_1}{x} \end{aligned}$$

$$= \frac{1}{y} + \frac{2c_1 y^{s_1+1} x^{-(s_1+2)}}{(s_1+1)(s_1+2)} \{1 + o(1)\} + \frac{2\theta_1}{x}.$$

By this result,

$$\begin{aligned} t \text{pr} \left(\frac{X_1^*}{b_1(t)} > x, \frac{X_2^*}{b_1(t)} = 0 \right) &= t \left\{ \text{pr} \left(X_2 < -\frac{1}{\log p} \right) - \text{pr} \left(X_1 < x b_1(t), X_2 < -\frac{1}{\log p} \right) \right\} \\ &= t \left(p - \exp \left[-V \{x b_1(t), (-\log p)^{-1}\} \right] \right) \\ &= t \left(p - p \exp \left[-\frac{2c_1 (-\log p)^{-(s_1+1)} \{x b_1(t)\}^{-(s_1+2)}}{(s_1+1)(s_1+2)} \{1 + o(1)\} - \frac{2\theta_1}{x b_1(t)} \right] \right) \\ &= t \left(p - p \left[1 - \frac{2c_1 (-\log p)^{-(s_1+1)} \{x b_1(t)\}^{-(s_1+2)}}{(s_1+1)(s_1+2)} + o \{b_1(t)^{-(s_1+2)}\} \right] \left[1 - \frac{2\theta_1}{x b_1(t)} + O \{b_1(t)^{-2}\} \right] \right) \\ &= \frac{t}{b_1(t)} \left(\frac{2\theta_1 p}{x} \right) \{1 + o(1)\} + \frac{t}{b_1(t)^{s_1+2}} \left\{ \frac{2c_1 p}{(s_1+1)(s_1+2)(-\log p)^{s_1+1} x^{s_1+2}} \right\} \{1 + o(1)\}. \end{aligned} \quad (25)$$

If $\theta_1 > 0$, i.e., there is extremal mass on $\{1\}$, we require that $t \asymp b_1(t)$ as $t \rightarrow \infty$, hence $\tau_1 = 1$. If $\theta_1 = 0$, we must have $t \asymp b_1(t)^{(s_1+2)}$ as $t \rightarrow \infty$, hence $\tau_1 = (s_1+2)^{-1}$. By similar calculations, if $h(w) \sim c_2 w^{s_2}$ as $w \rightarrow 0$ for $s_2 > -1$, we have $\tau_2 = 1$ if $\theta_2 > 0$, and $\tau_2 = (s_2+2)^{-1}$ otherwise. We now consider $\tau_{1,2}$. By homogeneity of the exponent measure, we have

$$\begin{aligned} t \text{pr} \left(\frac{X_1^*}{b_{1,2}(t)} > x, \frac{X_2^*}{b_{1,2}(t)} > y \right) &= t [1 - \text{pr}(X_1^* < x b_{1,2}(t)) - \text{pr}(X_2^* < y b_{1,2}(t)) + \text{pr}(X_1 < x b_{1,2}(t), X_2 < y b_{1,2}(t))] \\ &= t [1 - \exp \{-x^{-1} b_{1,2}(t)^{-1}\} - \exp \{-y^{-1} b_{1,2}(t)^{-1}\} + \exp \{-V(x, y) b_{1,2}(t)^{-1}\}] \\ &= t b_{1,2}(t)^{-1} \{x^{-1} + y^{-1} - V(x, y)\} + \frac{1}{2} t b_{1,2}(t)^{-2} \{V(x, y)^2 - x^{-2} - y^{-2}\} + O\{t b_{1,2}(t)^{-3}\}. \end{aligned}$$

If $V(x, y) \neq x^{-1} + y^{-1}$, then we require $b_{1,2}(t) \asymp t$, i.e., $\tau_{1,2} = 1$. Otherwise, if $V(x, y) = x^{-1} + y^{-1}$, corresponding to the independence case, we require that $b_{1,2}(t) \asymp t^{1/2}$ as $t \rightarrow \infty$, hence $\tau_{1,2} = 1/2$.

Acknowledgements

We gratefully acknowledge the support of the EPSRC funded STOR-i centre for doctoral training (E. Simpson) and an EPSRC fellowship (J. Wadsworth). We acknowledge the National River Flow Archive (NRFA) Centre for Ecology and Hydrology for use of the river flow and catchment boundary data. We thank the referees and associate editor for helpful comments that have improved the manuscript.

Supplementary Material

A Calculation of τ_C

A.1 Overview

In the Appendix, we derived τ_1 , τ_2 and $\tau_{1,2}$ for a particular subclass of bivariate extreme value distribution. Here, we investigate the case of the bivariate logistic distribution with all mass on the interior of the simplex, where p varies with t , and present further calculations of τ_C for several trivariate copula models.

A.2 Bivariate logistic distribution varying p

As stated in Section 2.3, we define τ_C in convergence (7) based upon X in that expression having marginal distribution (4) with p fixed. One could obtain alternative convergences like (7) by letting $p = p_t \rightarrow 1$ at a suitable rate, so that those variables in $D \setminus C$ are assumed to be growing at a slower rate than those in C . We illustrate this here, considering X_i^* defined as in (12), and taking $p_t = \exp\{-b_1(t)^{-\delta}\} = 1 - b_1(t)^{-\delta} \{1 + o(1)\}$ for $\delta \in (0, 1)$ so that

$$\text{pr} \left\{ \frac{X_1^*}{b_1(t)} > x, \frac{X_2^*}{b_1(t)} = 0 \right\} = \text{pr} \left\{ X_1 > b_1(t)x, X_2 < b_1(t)\delta \right\}.$$

To demonstrate this, we consider the bivariate logistic distribution: a special case of the bivariate extreme value distribution discussed previously.

The bivariate extreme value distribution with logistic structure has exponent measure

$$V(x, y) = \left(x^{-1/\alpha} + y^{-1/\alpha} \right)^\alpha,$$

for $x, y > 0$, and spectral density $h(w)$ given in (10). For $\alpha \in (0, 1)$, $H(\{0\}) = H(\{1\}) = 0$: we consider this case here. As $w \rightarrow 1$,

$$h(w) \sim \frac{1}{2} (\alpha^{-1} - 1) (1 - w)^{-2+1/\alpha},$$

which is equivalent to $s_1 = -2 + 1/\alpha$ in the formulation of the Appendix. By equation (25), we have

$$t \text{pr} \left\{ \frac{X_1^*}{b_1(t)} > x, \frac{X_2^*}{b_1(t)} = 0 \right\} = \frac{t}{b_1(t)^{1/\alpha}} \left\{ \frac{\alpha p_t}{x^{1/\alpha} (-\log p_t)^{-1+1/\alpha}} \right\} \{1 + o(1)\},$$

as $t \rightarrow \infty$.

Substituting $p_t = \exp\{-b_1(t)^{-\delta}\}$,

$$\begin{aligned} t \text{pr} \left\{ \frac{X_1^*}{b_1(t)} > x, \frac{X_2^*}{b_1(t)} = 0 \right\} &= \frac{t}{b_1(t)^{1/\alpha}} \left(\frac{\alpha [1 - b_1(t)^{-\delta} \{1 + o(1)\}]}{x^{1/\alpha} b_1(t)^{-\delta(-1+1/\alpha)}} \right) \{1 + o(1)\} \\ &= \frac{t}{b_1(t)^{1/\alpha + \delta - \delta/\alpha}} \left(\frac{\alpha}{x^{1/\alpha}} \right) \{1 + o(1)\}, \end{aligned}$$

hence taking $b_1(t) = t^{\alpha/(1-\delta+\delta\alpha)}$, we get convergence to a non-trivial form with $\tau_1 = \alpha/(1 - \delta + \delta\alpha)$. Thus, the index of hidden regular variation changes with the relative growth rates of X_1 and X_2 . Observe that for $\delta \rightarrow 0$, the value $\tau_1 = \alpha$ is recovered, whilst as $\delta \rightarrow 1$, the standard regular variation case is recovered.

A.3 Trivariate logistic distribution

The trivariate extreme value logistic distribution belongs to the class of trivariate extreme value distributions. The exponent measure of the logistic distribution has the form

$$V(x, y, z) = \left(x^{-1/\alpha} + y^{-1/\alpha} + z^{-1/\alpha} \right)^\alpha, \tag{26}$$

for $\alpha \in (0, 1]$. Since $\alpha = 1$ corresponds to the independence case, we restrict our calculations to $\alpha \in (0, 1)$. This distribution exhibits asymptotic dependence, with all extremal mass on the interior of the angular simplex, so $\tau_{1,2,3} = 1$. Our interest therefore lies with the values of τ_C on the vertices and edges of the simplex, and we consider each of these in turn.

Vertices: τ_1, τ_2, τ_3 . In a similar approach to the bivariate case, we calculate τ_1 by considering

$$\begin{aligned}
& \text{tpr} \left\{ \frac{X_1^*}{b_1(t)} > x, \frac{X_2^*}{b_1(t)} = 0, \frac{X_3^*}{b_1(t)} = 0 \right\} \\
&= t \left[\text{pr} \left(X_2 < -\frac{1}{\log p}, X_3 < -\frac{1}{\log p} \right) - \text{pr} \left\{ X_1 < xb_1(t), X_2 < -\frac{1}{\log p}, X_3 < -\frac{1}{\log p} \right\} \right] \\
&= t \left\{ \exp(2^\alpha \log p) - \exp \left(- \left[\{xb_1(t)\}^{-1/\alpha} + 2(-\log p)^{1/\alpha} \right]^\alpha \right) \right\} \\
&= t \left\{ p^{2^\alpha} - \exp \left(2^\alpha \log p \left[1 + \frac{\{xb_1(t)\}^{-1/\alpha}}{2(-\log p)^{1/\alpha}} \right]^\alpha \right) \right\} \\
&= t \left(p^{2^\alpha} - \exp \left[2^\alpha \log p - \frac{2^{\alpha-1} \alpha \{xb_1(t)\}^{-1/\alpha}}{(-\log p)^{-1+1/\alpha}} + O \left\{ b_1(t)^{-2/\alpha} \right\} \right] \right) \\
&= t \left(p^{2^\alpha} - p^{2^\alpha} \left[1 - \frac{2^{\alpha-1} \alpha \{xb_1(t)\}^{-1/\alpha}}{(-\log p)^{-1+1/\alpha}} + O \left\{ b_1(t)^{-2/\alpha} \right\} \right] \right) \\
&= tp^{2^\alpha} \left[\frac{2^{\alpha-1} \alpha \{xb_1(t)\}^{-1/\alpha}}{(-\log p)^{-1+1/\alpha}} + O \left\{ b_1(t)^{-2/\alpha} \right\} \right] \rightarrow \frac{2^{\alpha-1} p^{2^\alpha} \alpha x^{-1/\alpha}}{(-\log p)^{-1+1/\alpha}},
\end{aligned}$$

if $b_1(t) \sim t^\alpha$, which implies that $\tau_1 = \alpha$. By symmetry, we also have $\tau_2 = \tau_3 = \alpha$.

Edges: $\tau_{1,2}, \tau_{1,3}, \tau_{2,3}$. We carry out a similar calculation to find the value of $\tau_{1,2}$, corresponding to an edge of the triangular simplex. Here, we have

$$\begin{aligned}
& \text{tpr} \left\{ \frac{X_1^*}{b_{1,2}(t)} > x, \frac{X_2^*}{b_{1,2}(t)} > y, \frac{X_3^*}{b_{1,2}(t)} = 0 \right\} \\
&= t \left[\text{pr} \left(X_3 < -\frac{1}{\log p} \right) - \text{pr} \left\{ X_1 < xb_{1,2}(t), X_3 < -\frac{1}{\log p} \right\} - \text{pr} \left\{ X_2 < yb_{1,2}(t), X_3 < -\frac{1}{\log p} \right\} \right] \\
&\quad + \text{tpr} \left\{ X_1 < xb_{1,2}(t), X_2 < yb_{1,2}(t), X_3 < -\frac{1}{\log p} \right\} \\
&= t \left\{ p - \exp \left(\log p \left[1 + \frac{\{xb_{1,2}(t)\}^{-1/\alpha}}{(-\log p)^{1/\alpha}} \right]^\alpha \right) - \exp \left(\log p \left[1 + \frac{\{yb_{1,2}(t)\}^{-1/\alpha}}{(-\log p)^{1/\alpha}} \right]^\alpha \right) \right\} \\
&\quad + t \exp \left[\log p \left\{ 1 + \frac{b_{1,2}(t)^{-1/\alpha} (x^{-1/\alpha} + y^{-1/\alpha})}{(-\log p)^{1/\alpha}} \right\}^\alpha \right] \\
&= tp \left(1 - \left[1 - \frac{\alpha \{xb_{1,2}(t)\}^{-1/\alpha}}{(-\log p)^{-1+1/\alpha}} - \frac{\alpha(\alpha-1) \{xb_{1,2}(t)\}^{-2/\alpha}}{2(-\log p)^{-1+2/\alpha}} \right] \right) \\
&\quad - tp \left(\left[1 - \frac{\alpha \{yb_{1,2}(t)\}^{-1/\alpha}}{(-\log p)^{-1+1/\alpha}} - \frac{\alpha(\alpha-1) \{yb_{1,2}(t)\}^{-2/\alpha}}{2(-\log p)^{-1+2/\alpha}} \right] \right) \\
&\quad + tp \left\{ 1 - \frac{\alpha b_{1,2}(t)^{-1/\alpha} (x^{-1/\alpha} + y^{-1/\alpha})}{(-\log p)^{-1+1/\alpha}} - \frac{\alpha(\alpha-1) b_{1,2}(t)^{-2/\alpha} (x^{-1/\alpha} + y^{-1/\alpha})^2}{2(-\log p)^{-1+2/\alpha}} \right\} + O \left\{ tb_{1,2}(t)^{-3/\alpha} \right\} \\
&= b_{1,2}(t)^{-2/\alpha} t \left[\frac{p\alpha(\alpha-1)}{2(-\log p)^{-1+2/\alpha}} \left\{ x^{-2/\alpha} + y^{-2/\alpha} - (x^{-1/\alpha} + y^{-1/\alpha})^2 \right\} \right] + O \left\{ tb_{1,2}(t)^{-3/\alpha} \right\}
\end{aligned}$$

$$\rightarrow \frac{p\alpha(\alpha-1)}{2(-\log p)^{-1+2/\alpha}} \left\{ x^{-2/\alpha} + y^{-2/\alpha} - \left(x^{-1/\alpha} + y^{-1/\alpha} \right)^2 \right\},$$

if $b_{1,2}(t) \sim t^{\alpha/2}$, which implies that $\tau_{1,2} = \alpha/2$. Similarly, $\tau_{1,3} = \tau_{2,3} = \alpha/2$.

These calculations reveal different rates on the vertices and edges of the angular simplex in the trivariate logistic case.

A.4 Trivariate distribution with extremal mass on one vertex and one edge

Now we consider a trivariate example where the extremal mass is placed on one vertex and one edge of the triangular simplex. This can be achieved by taking (X_1, X_2) to have a bivariate extreme value logistic distribution, and X_3 to be a standard Fréchet random variable independent of (X_1, X_2) . The exponent measure in this case has the form

$$V(x, y, z) = \left(x^{-1/\alpha} + y^{-1/\alpha} \right)^\alpha + z^{-1},$$

for $\alpha \in (0, 1)$. We have $\tau_3 = \tau_{1,2} = 1$.

Vertices: τ_1, τ_2 . We first consider the vertex corresponding to only X_1 being large. Following a similar procedure as previously, and exploiting the independence of (X_1, X_2) and X_3 , we have

$$\begin{aligned} & \text{tpr} \left\{ \frac{X_1^*}{b_1(t)} > x, \frac{X_2^*}{b_1(t)} = 0, \frac{X_3^*}{b_1(t)} = 0 \right\} \\ &= \text{tpr} \left(X_3 < -\frac{1}{\log p} \right) \left[\text{pr} \left(X_2 < -\frac{1}{\log p} \right) - \text{pr} \left\{ X_1 < xb_1(t), X_2 < -\frac{1}{\log p} \right\} \right] \\ &= b_1(t)^{-1/\alpha} t \left\{ \frac{p^2 \alpha x^{-1/\alpha}}{(-\log p)^{-1+1/\alpha}} \right\} + O \left\{ tb_1(t)^{-2/\alpha} \right\} \rightarrow \frac{p^2 \alpha x^{-1/\alpha}}{(-\log p)^{-1+1/\alpha}}, \end{aligned}$$

if $b_1(t) \sim t^\alpha$, which implies that $\tau_1 = \alpha$. By similar calculations, $\tau_2 = \alpha$.

Edges: $\tau_{1,3}, \tau_{2,3}$. Next, we consider the edge of the angular simplex corresponding to only variables X_1 and X_3 being simultaneously large. In this case, we have

$$\begin{aligned} & \text{tpr} \left\{ \frac{X_1^*}{b_{1,3}(t)} > x, \frac{X_2^*}{b_{1,3}(t)} = 0, \frac{X_3^*}{b_{1,3}(t)} > z \right\} \\ &= \text{tpr} \{ X_3 > zb_{1,3}(t) \} \left[\text{pr} \left(X_2 < -\frac{1}{\log p} \right) - \text{pr} \left\{ X_1 < xb_{1,3}(t), X_2 < -\frac{1}{\log p} \right\} \right] \\ &= tp \left[\{ zb_{1,3}(t) \}^{-1} + O \{ b_{1,3}(t)^{-2} \} \right] \left[\frac{\alpha \{ xb_{1,3}(t) \}^{-1/\alpha}}{(-\log p)^{-1+1/\alpha}} + O \{ b_{1,3}(t)^{-2/\alpha} \} \right] \rightarrow \frac{p\alpha z^{-1} x^{-1/\alpha}}{(-\log p)^{-1+1/\alpha}}, \end{aligned}$$

if $b_{1,3}(t) \sim t^{\alpha/(1+\alpha)}$, which implies that $\tau_{1,3} = \alpha/(1+\alpha)$. Again by symmetry, $\tau_{2,3} = \alpha/(1+\alpha)$.

Interior: $\tau_{1,2,3}$. Finally, we consider the interior of the simplex, where

$$\begin{aligned} & \text{tpr} \left\{ \frac{X_1^*}{b_{1,2,3}(t)} > x, \frac{X_2^*}{b_{1,2,3}(t)} > y, \frac{X_3^*}{b_{1,2,3}(t)} > z \right\} \\ &= t \left[1 - \text{pr} \{ X_1 < xb_{1,2,3}(t) \} - \text{pr} \{ X_2 < yb_{1,2,3}(t) \} + \text{pr} \{ X_1 < xb_{1,2,3}(t), X_2 < yb_{1,2,3}(t) \} \right] \text{pr} \{ X_3 > zb_{1,2,3}(t) \} \\ &= t \left[b_{1,2,3}(t)^{-1} \left\{ x^{-1} + y^{-1} - \left(x^{-1/\alpha} + y^{-1/\alpha} \right)^\alpha \right\} + O \{ b_{1,2,3}(t)^{-2} \} \right] \left[\{ zb_{1,2,3}(t) \}^{-1} + O \{ b_{1,2,3}(t)^{-2} \} \right] \\ &= b_{1,2,3}(t)^{-2} t z^{-1} \left\{ x^{-1} + y^{-1} - \left(x^{-1/\alpha} + y^{-1/\alpha} \right)^\alpha \right\} + O \{ tb_{1,2,3}(t)^{-3} \} \\ &\rightarrow z^{-1} \left\{ x^{-1} + y^{-1} - \left(x^{-1/\alpha} + y^{-1/\alpha} \right)^\alpha \right\}, \end{aligned}$$

if $b_{1,2,3}(t) \sim t^{1/2}$, which implies that $\tau_{1,2,3} = 1/2$.

Illustration of Theorem 1. We can use this example to provide an illustration of Theorem 1. Variables X_1 and X_3 are independent, and therefore $\eta_{1,3} = 1/2$. By Theorem 1, we have

$$\eta_C = \max_{\bar{C}: C \subseteq \bar{C}} \tau_{\bar{C}}$$

for any $C \in 2^D \setminus \emptyset$. For $C = \{1, 3\}$, this corresponds to

$$\eta_{1,3} = \max \{\tau_{1,3}, \tau_{1,2,3}\} = \max \{1/2, \alpha/(1 + \alpha)\} = 1/2,$$

since $\alpha/(1 + \alpha) \in (0, 1/2)$ for $\alpha \in (0, 1)$.

A.5 Trivariate inverted logistic distribution

Next, we consider an inverted trivariate extreme value distribution, defined via its distribution function

$$\begin{aligned} \text{pr}\{X_1 < x, X_2 < y, X_3 < z\} &= 1 - \{F_X(x') + F_Y(y') + F_Z(z')\} \\ &\quad + \{F_{X,Y}(x', y') + F_{X,Z}(x', z') + F_{Y,Z}(y', z')\} - F_{X,Y,Z}(x', y', z'), \end{aligned}$$

where $F_{X,Y,Z}$ denotes the corresponding trivariate extreme value distribution function; $F_{X,Y}$, $F_{X,Z}$ and $F_{Y,Z}$ are the corresponding bivariate distribution functions; F_X , F_Y and F_Z are the marginal distributions of X , Y and Z ;

$$x' = -\frac{1}{\log(1 - e^{-1/x})} \sim \frac{1}{\log x},$$

as $x \rightarrow \infty$, and y' , z' are defined analogously. Note that if $x = -1/\log p$, $x' = -1/\log(1 - p)$. In the case of the trivariate inverted logistic distribution, which we focus on here, $F_{X,Y,Z}(x, y, z) = \exp\{-V(x, y, z)\}$, for V defined as in (26). The inverted logistic distribution has asymptotic independence, placing all extremal mass on the corners of the angular simplex, so $\tau_1 = \tau_2 = \tau_3 = 1$. We are therefore interested in calculating $\tau_{1,2,3}$, $\tau_{1,2}$, $\tau_{1,3}$ and $\tau_{2,3}$.

Interior: $\tau_{1,2,3}$. To calculate the index of hidden regular variation on the interior of the simplex, we consider

$$\begin{aligned} & \text{tpr} \left\{ \frac{X_1^*}{b_{1,2,3}(t)} > x, \frac{X_2^*}{b_{1,2,3}(t)} > y, \frac{X_3^*}{b_{1,2,3}(t)} > z \right\} \\ &= \text{tpr} \{X_1 > xb_{1,2,3}(t), X_2 > yb_{1,2,3}(t), X_3 > zb_{1,2,3}(t)\} \\ &= t \exp \left(-V \left[-\frac{1}{\log \{1 - e^{-x^{-1}b_{1,2,3}(t)^{-1}}\}}, -\frac{1}{\log \{1 - e^{-y^{-1}b_{1,2,3}(t)^{-1}}\}}, -\frac{1}{\log \{1 - e^{-z^{-1}b_{1,2,3}(t)^{-1}}\}} \right] \right) \\ &= t \exp \left\{ - \left(\left[-\log \{1 - e^{-x^{-1}b_{1,2,3}(t)^{-1}}\} \right]^{1/\alpha} + \left[-\log \{1 - e^{-y^{-1}b_{1,2,3}(t)^{-1}}\} \right]^{1/\alpha} + \left[-\log \{1 - e^{-z^{-1}b_{1,2,3}(t)^{-1}}\} \right]^{1/\alpha} \right)^\alpha \right\} \\ &= t \exp \left[- \left\{ (\log [xb_{1,2,3}(t)\{1 + o(1)\}])^{1/\alpha} + (\log [yb_{1,2,3}(t)\{1 + o(1)\}])^{1/\alpha} + (\log [zb_{1,2,3}(t)\{1 + o(1)\}])^{1/\alpha} \right\}^\alpha \right] \\ &= t \left[\exp \left\{ -\log [b_{1,2,3}(t)\{1 + o(1)\}] \left(3 + \frac{\log x + \log y + \log z}{\alpha \log [b_{1,2,3}(t)\{1 + o(1)\}]} \right)^\alpha \right\} \right] \\ &= tb_{1,2,3}(t)^{-3\alpha} \exp \left[-3^{\alpha-1} (\log x + \log y + \log z) \{1 + o(1)\} \right], \end{aligned}$$

so $b_{1,2,3}(t) \asymp t^{3-\alpha}$, which implies that $\tau_{1,2,3} = 3^{-\alpha}$. This corresponds to the known value of $\eta_{1,2,3}$ for the trivariate inverted logistic distribution, as $\eta_{1,2,3} = V(1, 1, 1)^{-1} = 3^{-\alpha}$.

Edges: $\tau_{1,2}$, $\tau_{1,3}$, $\tau_{2,3}$. We now consider the edge of the angular simplex corresponding to only variables X_1 and X_2 being simultaneously extreme, while X_3 is of smaller order. We have

$$\text{tpr} \left\{ \frac{X_1^*}{b_{1,2}(t)} > x, \frac{X_2^*}{b_{1,2}(t)} > y, \frac{X_3^*}{b_{1,2}(t)} = 0 \right\}$$

$$\begin{aligned}
&= \text{tpr} \left\{ X_1 > xb_{1,2}(t), X_2 > yb_{1,2}(t), X_3 < -\frac{1}{\log p} \right\} \\
&= t \left[\text{pr} \{X_1 > xb_{1,2}(t), X_2 > yb_{1,2}(t)\} - \text{pr} \left\{ X_1 > xb_{1,2}(t), X_2 > yb_{1,2}(t), X_3 > -\frac{1}{\log p} \right\} \right] \\
&= t \left(\exp \left[- \left\{ (\log[xb_{1,2}(t)\{1+o(1)\}])^{1/\alpha} + (\log[yb_{1,2}(t)\{1+o(1)\}])^{1/\alpha} \right\}^\alpha \right] \right. \\
&\quad \left. - t \left(\exp \left[- \left\{ (\log[xb_{1,2}(t)\{1+o(1)\}])^{-1/\alpha} + (\log[yb_{1,2}(t)\{1+o(1)\}])^{-1/\alpha} + \{-\log(1-p)\}^{1/\alpha} \right\}^\alpha \right] \right) \right] \\
&= t \left\{ \exp \left(-2^\alpha \log b_{1,2}(t) - 2^{\alpha-1} \log(xy) + O[\log\{b_{1,2}(t)\}^{-1}] \right) \right\} \left(1 - \exp \left[-\alpha 2^{\alpha-1} \frac{\{-\log(1-p)\}^{1/\alpha}}{\{\log b_{1,2}(t)\}^{-1+1/\alpha}} \right] \right) \\
&\sim \frac{b_{1,2}(t)^{-2^\alpha}}{\{\log b_{1,2}(t)\}^{-1+1/\alpha}} t \exp \left\{ -2^{\alpha-1} \log(xy) \right\} \alpha 2^{\alpha-1} \{-\log(1-p)\}^{1/\alpha} \\
&\rightarrow \exp \left\{ -2^{\alpha-1} \log(xy) \right\} \alpha 2^{\alpha-1} \{-\log(1-p)\}^{1/\alpha},
\end{aligned}$$

if

$$\frac{b_{1,2}(t)^{-2^\alpha}}{\{\log b_{1,2}(t)\}^{-1+1/\alpha}} t \rightarrow 1, \text{ as } t \rightarrow \infty.$$

Taking $b_{1,2}(t) = t^{2^{-\alpha}} (2^{-\alpha} \log t)^{2^{-\alpha}(1-1/\alpha)}$, we have

$$\begin{aligned}
\frac{b_{1,2}(t)^{-2^\alpha}}{\{\log b_{1,2}(t)\}^{-1+1/\alpha}} t &= \frac{\left\{ t^{2^{-\alpha}} (2^{-\alpha} \log t)^{2^{-\alpha}(1-1/\alpha)} \right\}^{-2^\alpha} t}{\left[\log \left\{ t^{2^{-\alpha}} (2^{-\alpha} \log t)^{2^{-\alpha}(1-1/\alpha)} \right\} \right]^{-1+1/\alpha}} \\
&= \frac{(2^{-\alpha} \log t)^{-1+1/\alpha}}{\left[2^{-\alpha} \log t + \log \left\{ (2^{-\alpha} \log t)^{2^{-\alpha}(1-1/\alpha)} \right\} \right]^{-1+1/\alpha}} \rightarrow 1,
\end{aligned}$$

as $t \rightarrow \infty$. As such, the index of regular variation is $\tau_{1,2} = 2^{-\alpha}$. By symmetry, $\tau_{1,3} = \tau_{2,3} = 2^{-\alpha}$.

A.6 Multivariate Gaussian distribution

The multivariate Gaussian provides a further example of a distribution which asymptotically places all mass on the vertices of the simplex. In the case where $d = 3$, for a multivariate Gaussian distribution with covariance matrix Σ , Nolde (2014), for example, shows that

$$\eta_{1,2,3} = (\mathbf{1}_3^T \Sigma^{-1} \mathbf{1}_3)^{-1}; \quad \eta_{i,j} = \left(\mathbf{1}_2^T \Sigma_{i,j}^{-1} \mathbf{1}_2 \right)^{-1}, \quad i < j \in \{1, 2, 3\},$$

where $\Sigma_{i,j}$ is the submatrix of Σ corresponding to variables i and j , and $\mathbf{1}_d \in \mathbb{R}^d$ is a vector of 1s.

The covariance matrix Σ may be written as

$$\Sigma = \begin{bmatrix} 1 & \rho_{12} & \rho_{13} \\ \rho_{12} & 1 & \rho_{23} \\ \rho_{13} & \rho_{23} & 1 \end{bmatrix} = \begin{bmatrix} \Sigma_{12} & B \\ B^T & 1 \end{bmatrix}, \quad \text{where } \Sigma_{12} = \begin{bmatrix} 1 & \rho_{12} \\ \rho_{12} & 1 \end{bmatrix} \text{ and } B = \begin{bmatrix} \rho_{13} \\ \rho_{23} \end{bmatrix}.$$

We note that since Σ and Σ_{12} are covariance matrices, they must be positive definite, with $\det(\Sigma) = 1 - \rho_{12}^2 - \rho_{13}^2 - \rho_{23}^2 + 2\rho_{12}\rho_{13}\rho_{23} > 0$ and $\det(\Sigma_{12}) = 1 - \rho_{12}^2 > 0$. The inverse of Σ is given by the block matrix

$$\Sigma^{-1} = \begin{bmatrix} \Sigma_{12}^{-1} + \Sigma_{12}^{-1} B (1 - B^T \Sigma_{12}^{-1} B)^{-1} B^T \Sigma_{12}^{-1} & -\Sigma_{12}^{-1} B (1 - B^T \Sigma_{12}^{-1} B)^{-1} \\ -(1 - B^T \Sigma_{12}^{-1} B)^{-1} B^T \Sigma_{12}^{-1} & (1 - B^T \Sigma_{12}^{-1} B)^{-1} \end{bmatrix},$$

so that

$$\mathbf{1}_3^T \Sigma^{-1} \mathbf{1}_3 = \mathbf{1}_2^T \Sigma_{12}^{-1} \mathbf{1}_2 + (1 - B^T \Sigma_{12}^{-1} B)^{-1} (1 - \mathbf{1}_2^T \Sigma_{12}^{-1} B - B^T \Sigma_{12}^{-1} \mathbf{1}_2 + \mathbf{1}_2^T \Sigma_{12}^{-1} B B^T \Sigma_{12}^{-1} \mathbf{1}_2)$$

$$\begin{aligned}
&= \mathbf{1}_2^T \Sigma_{12}^{-1} \mathbf{1}_2 + \frac{1 - \rho_{12}^2}{1 - \rho_{12}^2 - \rho_{13}^2 - \rho_{23}^2 + 2\rho_{12}\rho_{13}\rho_{23}} (1 - 2\mathbf{1}_2^T \Sigma_{12}^{-1} B + \mathbf{1}_2^T \Sigma_{12}^{-1} B B^T \Sigma_{12}^{-1} \mathbf{1}_2) \\
&= \mathbf{1}_2^T \Sigma_{12}^{-1} \mathbf{1}_2 + \frac{\det(\Sigma_{12})}{\det(\Sigma)} (1 - \mathbf{1}_2^T \Sigma_{12}^{-1} B)^2 \\
&= \mathbf{1}_2^T \Sigma_{12}^{-1} \mathbf{1}_2 + \frac{\det(\Sigma_{12})}{\det(\Sigma)} \left(1 - \frac{\rho_{13} + \rho_{23}}{1 + \rho_{12}}\right)^2 \geq \mathbf{1}_2^T \Sigma_{12}^{-1} \mathbf{1}_2,
\end{aligned}$$

with equality if and only if $1 + \rho_{12} = \rho_{13} + \rho_{23}$. By similar calculations,

$$\mathbf{1}_3^T \Sigma^{-1} \mathbf{1}_3 \geq \mathbf{1}_2^T \Sigma_{i,j}^{-1} \mathbf{1}_2, \quad i < j \in \{1, 2, 3\},$$

which suggests that

$$\eta_{1,2,3} \leq \eta_{i,j}, \quad i < j \in \{1, 2, 3\}.$$

Applying Theorem 2, for this trivariate case, if $1 + \rho_C \neq \sum_{C':|C'|=2, C' \neq C} \rho_{C'}$ for all $C \subset \{1, 2, 3\}$ with $|C| = 2$, then $\tau_C = \eta_C$ for any set $C \subseteq \{1, 2, 3\}$ with $|C| \geq 2$.

B Calculating the mass on each face for an asymmetric logistic model

Proposition 1. *For the d -dimensional asymmetric logistic model with exponent measure (23) and $\alpha_C \equiv \alpha \in (0, 1)$ for all $C \in 2^D \setminus \emptyset$,*

$$dp_C^{(d)} = \sum_{i \in C} \theta_{i,C},$$

where $p_C^{(d)}$ denotes the proportion of mass on the face with variables $\{X_i : i \in C\}$ simultaneously extreme.

Proof. Consider the exponent measure of the asymmetric logistic model $V(x)$ as a sum of functions $V_C(x_C)$, for $C \in 2^D \setminus \emptyset$, i.e.,

$$V(x) = \sum_{C \in 2^D \setminus \emptyset} V_C(x_C), \quad V_C(x_C) = \left\{ \sum_{i \in C} \left(\frac{\theta_{i,C}}{x_i} \right)^{1/\alpha} \right\}^\alpha.$$

Then for any dimension $d \geq |C|$,

$$V^{\{C\}}(x_C) = \left(\prod_{i \in C} \frac{\partial}{\partial x_i} \right) V_C(x_C) = \left\{ \prod_{i=0}^{|C|-1} - \left(\frac{\alpha - i}{\alpha} \right) \right\} \left(\prod_{i \in C} \frac{\theta_{i,C}^{1/\alpha}}{x_{C,i}^{1+1/\alpha}} \right) \left\{ \sum_{i \in C} \left(\frac{\theta_{i,C}}{x_{C,i}} \right)^{1/\alpha} \right\}^{\alpha - |C|},$$

since for $\bar{C} \supset C$, $\lim_{x_i \rightarrow 0: i \in \bar{C} \setminus C} \left(\prod_{j \in \bar{C}} \frac{\partial}{\partial x_j} \right) V_{\bar{C}}(x_{\bar{C}}) = 0$. Hence, by result (22),

$$dp_C^{(d)} = - \int_{\mathbb{B}_C} V^{\{C\}}(w_C) \prod_{i \in C} dw_i, \quad (27)$$

which we note does not depend on d . We claim that

$$- \int_{\mathbb{B}_C} V^{\{C\}}(w_C) \prod_{i \in C} dw_i = \sum_{i \in C} \theta_{i,C}. \quad (28)$$

First consider $|C| = 1$, i.e. $\mathbb{B}_C = \{w : w_i = 1\}$ for $C = \{i\}$. Here,

$$V^{\{i\}}(x_i) = \frac{\partial}{\partial x_i} V_i(x_i) = - \frac{\theta_{i,i}}{x_i^2},$$

so

$$dp_i^{(d)} = \frac{\theta_{i,i}}{w_i^2} \Big|_{w_i=1} = \theta_{i,i}, \quad i = 1, \dots, d.$$

Now consider $|C| = 2$. We have

$$V^{\{i,j\}}(x_i, x_j) = \left(\frac{\alpha - 1}{\alpha}\right) \frac{\{(1 - \theta_{i,i})(1 - \theta_{j,j})\}^{1/\alpha}}{(x_i x_j)^{1+1/\alpha}} \left\{ \left(\frac{\theta_{i,ij}}{x_i}\right)^{1/\alpha} + \left(\frac{\theta_{j,ij}}{x_j}\right)^{1/\alpha} \right\}^{\alpha-2},$$

so

$$h_{i,j}(w_i) = \left(\frac{1 - \alpha}{\alpha}\right) \frac{(\theta_{i,ij}\theta_{j,ij})^{1/\alpha}}{\{w_i(1 - w_i)\}^{1+1/\alpha}} \left\{ \left(\frac{\theta_{i,ij}}{w_i}\right)^{1/\alpha} + \left(\frac{\theta_{j,ij}}{1 - w_i}\right)^{1/\alpha} \right\}^{\alpha-2},$$

and

$$dp_{i,j}^{(d)} = \int_0^1 h_{i,j}(w_i) dw_i. \quad (29)$$

However, taking $d = 2$, we know $2p_{1,2}^{(2)} + 2p_1^{(2)} + 2p_2^{(2)} = 2$, so $dp_{1,2}^{(d)} = \theta_{1,12} + \theta_{2,12}$, and similarly, by (29), $\int_0^1 h_{i,j}(w_i) dw_i = dp_{i,j}^{(d)} = \theta_{i,ij} + \theta_{j,ij}$. So, (27) holds for $|C| = 1$ and $|C| = 2$, and we suppose it holds for $|C| \leq k$, i.e. $dp_C^{(d)} = -\int_{\mathbb{B}_C} V^{\{C\}}(w_C) \prod_{i \in C} dw_i = \sum_{i \in C} \theta_{i,C}$.

Since (27) does not depend on d , take $d = k + 1$. So for all \underline{C} with $|\underline{C}| \leq k$, $(k + 1)p_{\underline{C}}^{(k+1)} = \sum_{i \in \underline{C}} \theta_{i,\underline{C}}$. Now take $C = \{1, \dots, k + 1\}$. Then,

$$\begin{aligned} (k + 1)p_C^{(k+1)} &= (k + 1) - \sum_{\underline{C} \subset C} \sum_{i \in \underline{C}} \theta_{i,\underline{C}} = (k + 1) - \sum_{i \in C} \sum_{\underline{C} \subset C} \theta_{i,\underline{C}} \\ &= \sum_{i \in C} \left(1 - \sum_{\underline{C} \subset C} \theta_{i,\underline{C}} \right) \\ &= \sum_{i \in C} \theta_{i,C}. \end{aligned}$$

As such, (28) holds by induction. □

C Simulation study

C.1 AUC results for the asymmetric logistic distribution

In Table 2 of the main paper, we present the average area under the ROC curve for the Method 1, Method 2 and the approach of Goix et al. applied to samples taken from various asymmetric logistic distributions. Figures 6 and 7 provide boxplots of all the AUC values obtained in these simulations. As was the case when comparing average AUC values, Method 1 and the approach of Goix et al. (2017) perform similarly, and better than Method 2, particularly for cases where the dependence parameter α is 0.25 or 0.5. For $\alpha = 0.75$, the approach of Goix et al. generally performs better than our two methods.

C.2 Additional Hellinger results for the asymmetric logistic distribution

In Figure 8, we present Hellinger distance results for the two cases omitted from the paper; $(n, d, f) = (10000, 5, 10)$ and $(n, d, f) = (100000, 10, 50)$.

C.3 A max-mixture distribution

Segers (2012) shows how to construct distributions that place extremal mass on different combinations of faces of the angular unit simplex. Here, we take a different approach by considering max-mixture models. The asymmetric logistic example of Section 4.2 can be thought of as a max-mixture distribution whose components either exhibit asymptotic dependence or have complete independence. It is also of interest to consider models

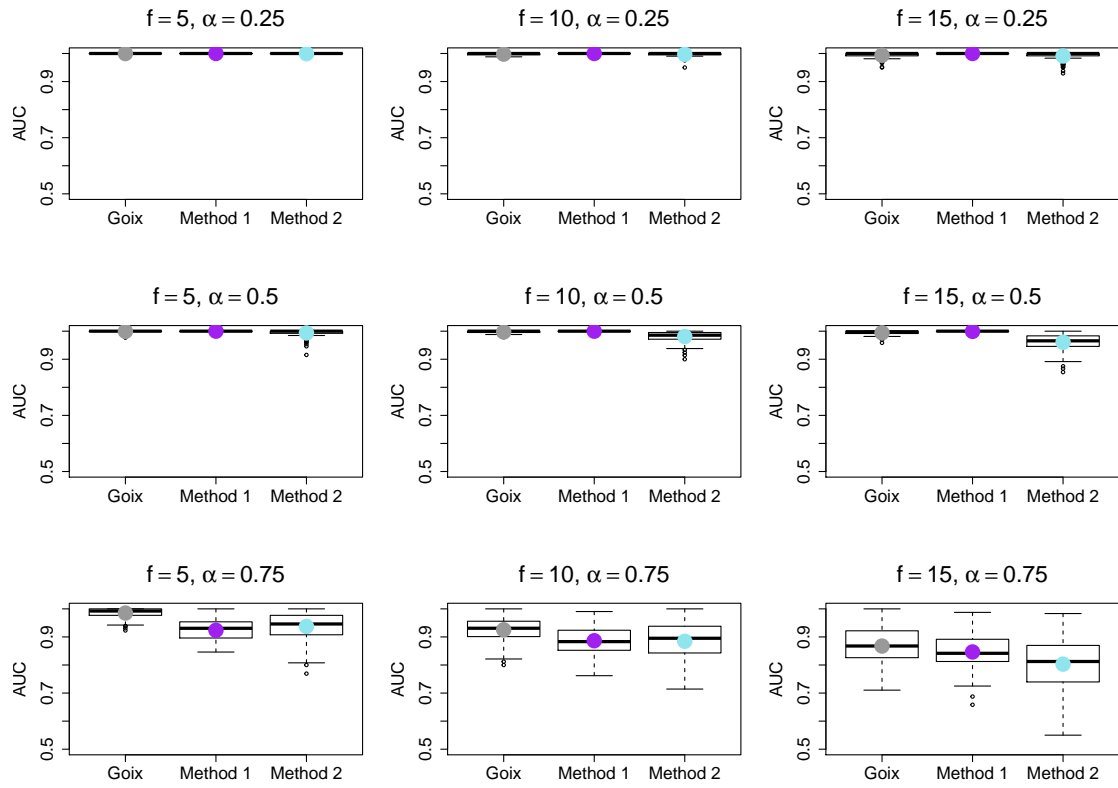


Figure 6: AUC results for 100 simulations from a five dimensional asymmetric logistic distribution.

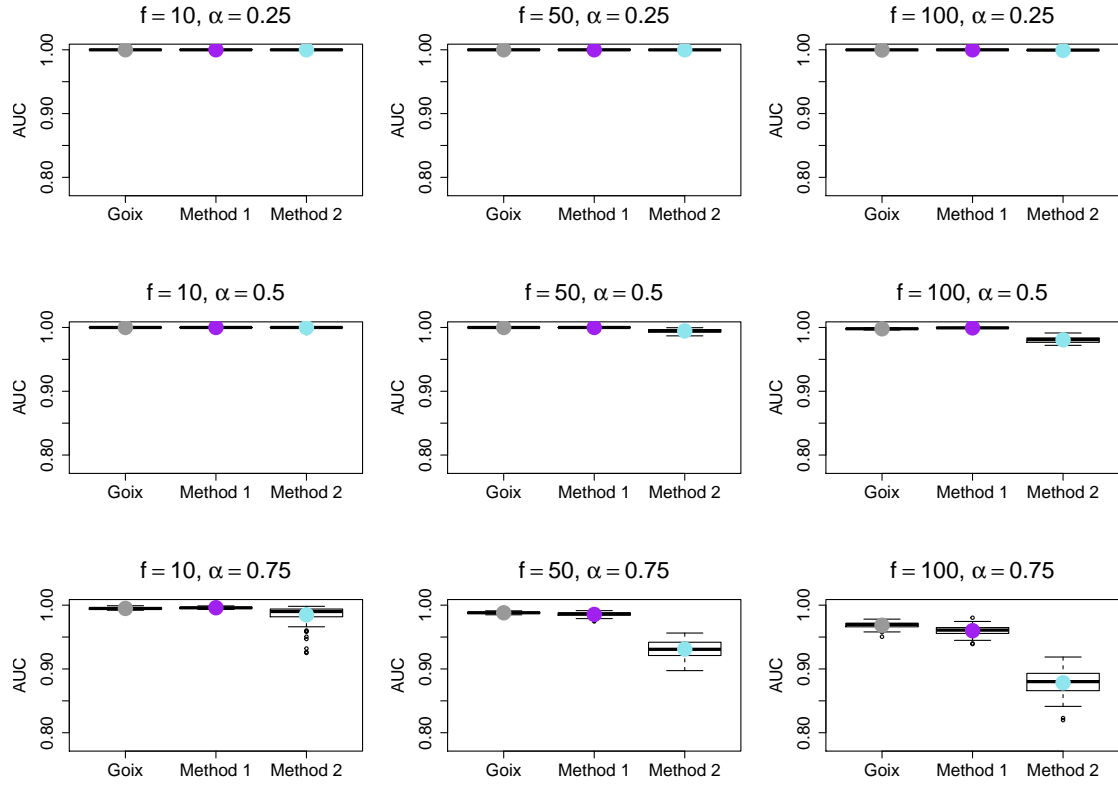


Figure 7: AUC results for 100 simulations from a ten dimensional asymmetric logistic distribution.

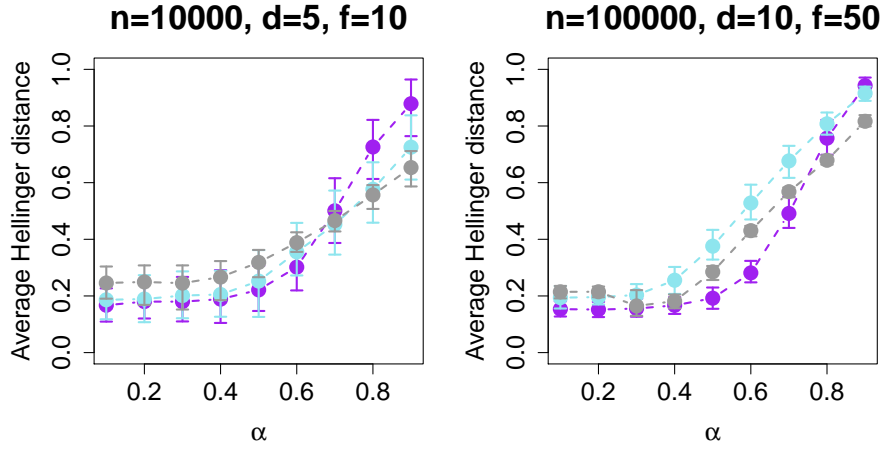


Figure 8: Mean Hellinger distance, 0.05 and 0.95 quantiles over 100 simulations. Method 1: purple; Method 2: blue; Goix et al.: grey.

with some components exhibiting overall dependence, but independence in the tails. Such a model can be constructed using a mixture of extreme value logistic and multivariate Gaussian copulas, a particular example of which we consider here.

Let $Z_C = (Z_{j,C} : j \in C)$ be a $|C|$ -dimensional random vector with standard Fréchet marginal distributions, and $\{Z_C : C \in 2^D \setminus \emptyset\}$ be independent random vectors. Define the vector $X = (X_1, \dots, X_d)$ with components

$$X_i = \max_{C \in 2^D \setminus \emptyset : j \in C} (\theta_{j,C} Z_{j,C}); \quad \theta_{j,C} \in [0, 1]; \quad \sum_{C \in 2^D \setminus \emptyset : j \in C} \theta_{j,C} = 1,$$

for $i = 1, \dots, d$. The random vector Z_C may exhibit asymptotic dependence, in which case mass will be placed on the interior of the face of the angular simplex corresponding to all variables in $\{X_i : i \in C\}$ being simultaneously large, or it may exhibit asymptotic independence, in which case mass will be placed on the vertices of that face.

Here, we consider one particular 5-dimensional example. We define

- $Z_{\{1,2\}}$ and $Z_{\{4,5\}}$ as following bivariate Gaussian copulas with correlation parameter ρ ;
- $Z_{\{1,2,3\}}$, $Z_{\{3,4,5\}}$ and $Z_{\{1,2,3,4,5\}}$ as having 3- and 5- dimensional extreme value logistic copulas with dependence parameter α .

The bivariate Gaussian distribution is asymptotically independent, while the logistic distribution is asymptotically dependent for $\alpha \in (0, 1)$. As such, the faces with mass resulting from this construction are those corresponding to the sets of variables $\{X_1, X_2, X_3\}$, $\{X_3, X_4, X_5\}$ and $\{X_1, X_2, X_3, X_4, X_5\}$ being simultaneously large while the other variables are of smaller order, and there will also be extremal mass on some vertices of the simplex, corresponding to variables $\{X_1\}$, $\{X_2\}$, $\{X_4\}$ and $\{X_5\}$ being large individually. We assign equal mass to each of these seven faces by setting

$$\begin{aligned} \theta_{\{1,2\}} = (\theta_{1,\{1,2\}}, \theta_{2,\{1,2\}}) &= (5, 5) / 7, & \theta_{\{4,5\}} &= (5, 5) / 7, & \theta_{\{1,2,3\}} &= (1, 1, 3) / 7, \\ \theta_{\{3,4,5\}} &= (3, 1, 1) / 7, & \theta_{\{1,2,3,4,5\}} &= (1, 1, 1, 1, 1) / 7. \end{aligned}$$

As in the 5-dimensional asymmetric logistic case, we take a sample of size 10,000 and compare Methods 1 and 2 to the approach of Goix et al. (2017). We set the tuning parameters as in Section 4.2 of the paper. The average results of 100 such tests are demonstrated in Figure 9, where we show the mean Hellinger distance

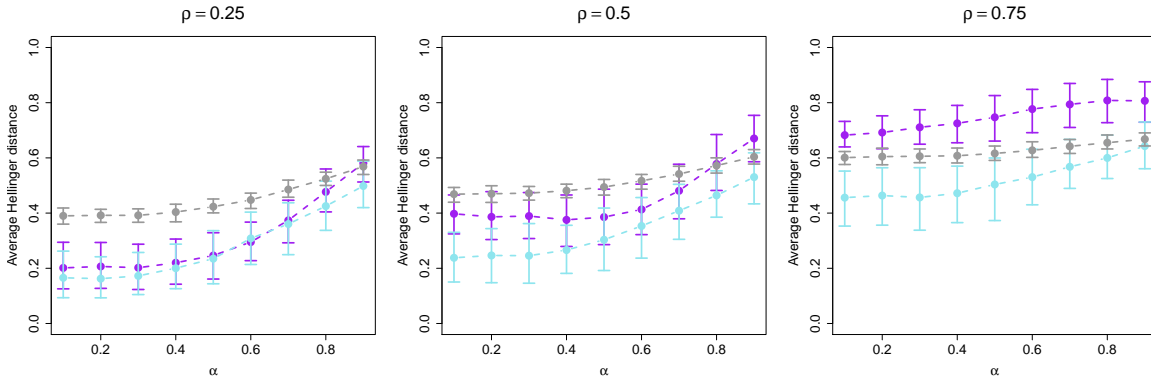


Figure 9: Mean Hellinger distance, 0.05 and 0.95 quantiles over 100 simulations. Method 1: purple; Method 2: blue; Goix et al.: grey.

(α, ρ)	(0.25, 0.25)	(0.25, 0.5)	(0.25, 0.75)	(0.5, 0.25)	(0.5, 0.5)	(0.5, 0.75)	(0.75, 0.25)	(0.75, 0.5)	(0.75, 0.75)
Goix et al.	0.997	0.922	0.912	0.997	0.920	0.906	0.962	0.900	0.878
Method 1	1.000	0.973	0.930	0.999	0.965	0.900	0.964	0.914	0.875
Method 2	0.999	0.992	0.939	0.995	0.984	0.922	0.953	0.937	0.866

Table 5: Average AUC values for 100 samples from a 5-dimensional mixture of bivariate Gaussian and extreme value logistic distributions.

for $\alpha \in [0.1, 0.9]$, and for values of the bivariate Gaussian correlation $\rho \in \{0.25, 0.5, 0.75\}$.

In terms of the Hellinger distance, Method 2 clearly out-performs the method of Goix et al. and our Method 1. The performance of all three methods deteriorates as the value of the correlation parameter ρ increases, and there is some increase in the average Hellinger distance as the logistic dependence parameter increases, although it is reasonably stable for values of α between 0.1 and 0.5.

The AUC values in Table 5 focus on $\alpha, \rho \in \{0.25, 0.5, 0.75\}$. As with the Hellinger distance, we see that the methods both perform worse in the case where $\alpha = 0.75$, while all methods perform particularly well when $\rho = 0.25$, corresponding to quite weak correlation. Again, as the value of the correlation parameter ρ is increased, the area under the curves becomes smaller, but the results are still promising for our methods in these cases. For $\rho = 0.25$, Method 1 always performs the best, while for $\rho = 0.5$ and $\rho = 0.75$, Method 2 is generally most successful.

References

- Asadi, P., Davison, A. C., and Engelke, S. (2015). Extremes on river networks. *The Annals of Applied Statistics*, 9(4):2023–2050.
- Chautru, E. (2015). Dimension reduction in multivariate extreme value analysis. *Electron. J. Statist.*, 9(1):383–418.
- Chiapino, M. and Sabourin, A. (2017). Feature clustering for extreme events analysis, with application to extreme stream-flow data. In *New Frontiers in Mining Complex Patterns*, pages 132–147, Cham. Springer International Publishing.
- Chiapino, M., Sabourin, A., and Segers, J. (2018). Identifying groups of variables with the potential of being large simultaneously. *arXiv:1802.09977*.

- Coles, S. G. and Tawn, J. A. (1991). Modelling extreme multivariate events. *Journal of the Royal Statistical Society: Series B (Methodological)*, 53(2):377–392.
- Das, B., Mitra, A., and Resnick, S. (2013). Living on the multidimensional edge: Seeking hidden risks using regular variation. *Advances in Applied Probability*, 45(01):139–163.
- Goix, N., Sabourin, A., and Cl  men  on, S. (2016). Sparse representation of multivariate extremes with applications to anomaly ranking. *Proceedings of the 19th International Conference on Artificial Intelligence and Statistics*, 51:75–83.
- Goix, N., Sabourin, A., and Cl  men  on, S. (2017). Sparse representation of multivariate extremes with applications to anomaly detection. *Journal of Multivariate Analysis*, 161:12–31.
- Hastie, T., Tibshirani, R., and Friedman, J. H. (2009). *The Elements of Statistical Learning: Data Mining, Inference, and Prediction*. Springer Series in Statistics. Springer, New York, 2nd edition.
- Heffernan, J. E. and Tawn, J. A. (2004). A conditional approach for multivariate extreme values (with discussion). *Journal of the Royal Statistical Society: Series B (Statistical Methodology)*, 66(3):497–546.
- Hill, B. M. (1975). A simple general approach to inference about the tail of a distribution. *The Annals of Statistics*, 3(5):1163–1174.
- Hua, L. and Joe, H. (2011). Tail order and intermediate tail dependence of multivariate copulas. *Journal of Multivariate Analysis*, 102(10):1454–1471.
- Keef, C., Tawn, J. A., and Lamb, R. (2013). Estimating the probability of widespread flood events. *Environmetrics*, 24(1):13–21.
- Kl  ppelberg, C., Haug, S., and Kuhn, G. (2015). Copula structure analysis based on extreme dependence. *Statistics and its Interface*, 8(1):93–107.
- Ledford, A. W. and Tawn, J. A. (1996). Statistics for near independence in multivariate extreme values. *Biometrika*, 83(1):169–187.
- Ledford, A. W. and Tawn, J. A. (1997). Modelling dependence within joint tail regions. *Journal of the Royal Statistical Society: Series B (Statistical Methodology)*, 59(2):475–499.
- Maulik, K. and Resnick, S. (2004). Characterizations and examples of hidden regular variation. *Extremes*, 7(1):31–67.
- Mitra, A. and Resnick, S. (2011). Hidden regular variation and detection of hidden risks. *Stochastic Models*, 27(4):591–614.
- Morris, D. G. and Flavin, R. W. (1990). A digital terrain model for hydrology. *Proc 4th International Symposium on Spatial Data Handling*, 1:250–262.
- Morris, D. G. and Flavin, R. W. (1994). Sub-set of UK 50m by 50m hydrological digital terrain model grids. *NERC, Institute of Hydrology, Wallingford*.
- Nolde, N. (2014). Geometric interpretation of the residual dependence coefficient. *Journal of Multivariate Analysis*, 123:85–95.
- Resnick, S. I. (2002). Hidden regular variation, second order regular variation and asymptotic independence. *Extremes*, 5(4):303–336.
- Resnick, S. I. (2010). *Heavy-Tail Phenomena: Probabilistic and Statistical Modeling*. Springer Series in Operations Research.
- Segers, J. (2012). Max-stable models for multivariate extremes. *REVSTAT*, 10(1):61–82.

- Tawn, J. A. (1988). Bivariate extreme value theory: Models and estimation. *Biometrika*, 75(3):397–415.
- Tawn, J. A. (1990). Modelling multivariate extreme value distributions. *Biometrika*, 77(2):245–253.
- Vettori, S., Huser, R., Segers, J., and Genton, M. G. (2017). Bayesian clustering and dimension reduction in multivariate extremes. *arXiv:1705.10488*.
- Wadsworth, J. L. and Tawn, J. A. (2013). A new representation for multivariate tail probabilities. *Bernoulli*, 19(5B):2689–2714.